UNIVERSITY OF CALIFORNIA SAN DIEGO

Subcellular Resolution Imaging of Lipid and Protein Metabolism in Cancer Cells Regulated with Amino Acids

A Thesis submitted in partial satisfaction of the requirements
for the degree Master of Science

in

Bioengineering

by

Pegah Bagheri

Committee in charge:

Professor Lingyan Shi, Chair
Professor Pedro Cabrales
Professor Geert W Schmid-Schoenbein

2022

The Thesis of Pegah Bagheri is approved, and it is acceptable in quality and form for publication on microfilm and electronically.

University of California San Diego

2022

DEDICATION

To my parents, who have always supported me and encouraged me to go on new adventures, and my sister, who has always inspired me to push past limits and reach new heights.

TABLE OF CONTENTS

LIST OF FIGURES

ACKNOWLEDGEMENTS

I would like to acknowledge Professor Lingyan Shi for her support as the chair of my committee. Professor Shi has been an invaluable mentor, and her guidance has ignited my passion for research and engineering that has led me to pursue a Doctor of Philosophy in bioengineering. This thesis would not be possible without the independence she granted me to pursue my own research interest and the encouragement she has kindly offered.

I thank Professor Pedro Cabrales and Professor Geert Schmid-Schoenbein for serving as my committee members. I would like to thank Dr. Yajuan Li, Dr. Hongje Jang, Anthony Fung, Khang Hoang, and everyone else in the Shi lab for being great mentors and colleagues. The knowledge and perspective that they provided was crucial for supporting my research development.

Finally, I would like to thank my family for all their love and support over these two years. Their moral support and consistent comfort have allowed me to follow my passion which I will always be forever grateful for.

Chapter 1, in full, is a reprint of the material as it appears in Visualizing Cancer Cell Metabolic Dynamics Regulated with Aromatic Amino Acids Using DO-SRS and 2PEF Microscopy 2021. Bagheri, P., Hoang, K., Fung, A.A, Hussain, S., & Shi, L. Frontiers in Molecular Biosciences, 8, 779702. https://doi.org/10.3389/fmolb.2021.779702. The thesis author was the primary investigator and author of this paper.

Chapter 2, in full, is currently being prepared for submission for publication of the material. Bagheri, P.; Shi, L. The thesis author was the primary investigator and author of this material.

ABSTRACT OF THE THESIS

Subcellular Resolution Imaging of Lipid and Protein Metabolism in Cancer Cells Regulated with Amino Acids

by

Pegah Bagheri

Master of Science in Bioengineering

University of California San Diego, 2022

Professor Lingyan Shi, Chair

Macromolecules, such as lipids and proteins, are key players in metabolic pathways related to cancer diseases. The synthesis of these macromolecules is related to the levels of amino acids in cells. Both essential and nonessential amino acids are considered to affect cancer cell survival and growth. Optical techniques that are both high resolution and non-destructive on the sample can aid in the understanding of metabolic changes in cancer cells. The objectives of this thesis are to provide insights into the effects of aromatic amino acids and nonessential amino acid (serine) on metabolic activities in cancer cells, by using Raman scattering microscopy for *in situ* subcellular imaging. The first chapter of this thesis presents a study on the influence of aromatic amino acids on lipid and protein metabolism in cancer cells using deuterium-oxide probed stimulated Raman scattering (SRS) and two-photon fluorescence

microscopy. The second chapter presents work investigating the effects of the nonessential amino acid (serine) on lipid and protein metabolism in cancer cells using SRS imaging. The data and results presented in this thesis provide insights into the implications of essential and nonessential amino acids manipulations in cancer metabolism and application of Raman imaging techniques as a potential early diagnostic tool for cancers.

INTRODUCTION

Understanding how cancer metabolism is affected has become a progressing topic that continues to influence the field of oncology. Typically, the focus of cancer metabolism lies in the central carbon metabolism such as the tricarboxylic acid cycle and glycolysis; however, new studies are emerging on the importance of amino acids impact on cancer metabolism (Lieu, Nguyen et al. 2020). Amino acids are organic compounds that are essential for homeostatic maintenance, redox balance, and energetic regulation (Takahara, Amemiya et al. 2020, Wei, Liu et al. 2020). They can either be synthesized in the body where these amino acids are considered to be nonessential, or obtained through the diet that are known as essential amino acids. Indeed, amino acids have shown to produce byproducts, such as lipids and proteins, and recent research has demonstrated the relevance of lipid and protein metabolism in cancer progression (Pavlova and Thompson 2016, Maddocks, Athineos et al. 2017, Mossmann, Park et al. 2018, Lieu, Nguyen et al. 2020, Takahara, Amemiya et al. 2020, Wei, Liu et al. 2020). It is important to analyze lipids in various scales in cancer cells and have the ability to image them *in situ*. Imaging is a fundamental tool in lipid studies that can provide essential information on cells without damaging or requiring too much sample preparation time. Being able to diagnose such metabolic changes in early cancer stages can allude to higher rate of cancer treatment and patient survival.

Many imaging techniques have the capability to observe small molecules that are usually based on fluorescence microscopy with the use of exogenous chemical probes. Mass spectrometry (MS)-based methods, gas chromatography (GC), or matrix-assisted laser desorption/ionization (MALDI)-MS imaging are examples of common analytical and imaging approaches for lipidomic studies (Murphy, Hankin et al. 2009, Pirman, Efuet et al. 2013, Di Gialleonardo, Wilson et al. 2016, Bowman, Bogie et al. 2020, Li, Cheng et al. 2021). However, these processes require either

long sample preparation time that can be destructive to cells, or fluorescent dyes that can disturb the molecular cell activities or have low spatial resolution. It is clear that there are many challenging aspects in these standard tools.

High-resolution, non-invasive optical techniques such as Raman scattering microscopy has emerged in the past decade for subcellular imaging in cells, tissues, and animals *in situ* (Fung and Shi 2020). The specific type of molecular bonds has a frequency of vibration correlated where the vibration of intensity can be recorded in the spectrum, and molecular bonds can be identified (Min, Freudiger et al. 2011). The Raman shift, which is generated from the energy difference between the incident and scattered light, is reflected by the vibrations of the molecular bonds' energy requirements (Min, Freudiger et al. 2011, Fung and Shi 2020). The high intensity shown in a spectrum at a particular frequency demonstrates a particular molecular bond.

Raman spectroscopy and microscopy are originally label-free, without the need of dyes or toxic labels (Shi, Shen et al. 2018, Shi, Zheng et al. 2018, Li, Zhang et al. 2021, Li, Bagheri et al. 2022). Studies have indicated metabolites related to lipid and protein metabolism in cancer are dependent on amino acids and have demonstrated connections between cancer progression and lipid and protein metabolism (Galbraith and Buse 1981, Pavlova and Thompson 2016, Gao, Lee et al. 2018). Raman spectroscopy and stimulated Raman scattering microscopy, coupled with heavy water (D_2O) probing, can visualize metabolic dynamics of biomolecules such as lipids, proteins, and DNA in cells (Shi, Shen et al. 2018, Shi, Zheng et al. 2018, Li, Zhang et al. 2021, Li, Bagheri et al. 2022). This imaging method can essentially detect newly-synthesized macromolecules, such as lipids and proteins, for understanding how changes in amino acids influence the turnover of these macromolecules in cancer cells. The objective of this thesis is to provide insights into the lipid and protein metabolism in cancer cells regulated with both essential

and nonessential amino acids using non-destructive imaging techniques: the spontaneous Raman spectroscopy, stimulated Raman scattering (SRS) microscopy, and two-photon excitation fluorescence (2PEF) microscopy.

The first chapter examines the effects of aromatic amino acids on lipid metabolism in HeLa cells using SRS and 2PEF imaging methods. We evaluated the hypothesis that excess aromatic amino acids, specifically phenylalanine and tryptophan, will upregulate lipid synthesis and induce mitochondrial damage, ultimately resulting in the accumulation of reactive oxygen species (ROS). By adding 15x phenylalanine and tryptophan to cell culture media, we investigated the relationship between the need of essential amino acids and cancer cell growth and survival using deuterium-oxide probed SRS (DO-SRS) imaging. The data presented in this chapter provide insight into how specific phenotypes and even minimal changes in cell metabolic activities can be used as potential indicators for early diagnostic methods for cancer and other closely related diseases. The study demonstrates the useful applications of DO-SRS and 2PEF microscopy to visualize in vitro changes with high resolution and without the need of labeling dyes, which can be translated to the optimization of current diagnostic tools used for diseases like cancer and neurodegeneration.

The second chapter investigates the effects of the nonessential amino acid (serine) on cancer cell metabolism, particularly lipid and protein metabolism, using DO-SRS and label-free SRS techniques. The results from this study have clinical implications on the changes in de novo lipid and protein synthesis when minimal and excess exogenous serine is added to cell culture media. An upregulation of serine correlates with an increase in lipogenesis and protein synthesis, implicating cancer cell growth and survival. When serine was deprived from cells, the lipid and protein metabolism experienced opposite effects compared to a surplus of serine, indicating that lack of serine can lead to accumulation of ROS and even cell death. Previous evidence has

indicated that tumors cannot acquire a viable amount of serine from their environment, and our study proved that varying serine concentration can influence the cell metabolism greatly in a very short time period. Raman and DO-SRS imaging techniques demonstrated that biomolecules, such as lipids and proteins, can be critical indicators to measure disease progression. Moreover, these potential methods allow us to observe and understand how amino acids, both essential and nonessential, can directly change the cell's metabolic activity, unraveling how lipids and proteins are influenced in a disease state.

CHAPTER 1. VISUALIZING CANCER CELL METABOLIC DYNAMICS REGULATED WITH AROMATIC AMINO ACIDS USING DO-SRS AND 2PEF MICROSCOPY

Abstract: Oxidative imbalance plays an essential role in the progression of many diseases that include cancer and neurodegenerative diseases (Moneim 2015, Saha, Lee et al. 2017). Aromatic amino acids (AAA) such as phenylalanine and tryptophan have the capability of escalating oxidative stress because of their involvement in the production of Reactive Oxygen Species (ROS) (Kimura and Watanabe 2016). Here, we use D_2O (heavy water) probed stimulated Raman scattering microscopy (DO-SRS) and two Photon Excitation Fluorescence (2PEF) microscopy as a multimodal imaging approach to visualize metabolic changes in HeLa cells under excess AAA such as phenylalanine or trytophan in culture media. The cellular spatial distribution of de novo lipogenesis, new protein synthesis, NADH, Flavin, unsaturated lipids, and saturated lipid were all imaged and quantified in this experiment. Our studies reveal ~10% increase in de novo lipogenesis and the ratio of NADH to flavin, and ~50% increase of the ratio of unsaturated lipids to saturated lipid in cells treated with excess phenylalanine or trytophan. In contrast, these cells exhibited a decrease in the protein synthesis rate by ~10% under these AAA treatments. The cellular metabolic activities of these biomolecules are indicators of elevated oxidative stress and mitochondrial dysfunction. Furthermore, 3D reconstruction images of lipid droplets were acquired and quantified to observe their spatial distribution around cells' nuceli under different AAA culture media. We observed a higher proportion of lipid droplets in excess AAA conditions. Our study showcases that DO-SRS imaging can be used to quantitatively study how excess AAA regulates metabolic activities of cells with subcellular resolution *in situ*.

1.1 Introduction

The aromatic amino acids (AAA), L-phenylalanine and L-tryptophan, are essential for protein synthesis (Parthasarathy, Cross et al. 2018), serve as functional components in the regulation of many metabolic pathways (Wu 2013) with implications in diseases such as cancer (Cheng, Zhuo et al. 2019, Ma, Chen et al. 2021). AAAs can be critical intermediates that connect nucleotide, glucose, and lipid metabolism (Wei, Liu et al. 2020), but may also serve as energy sources for proliferating cancer cells. Oxidative imbalance and stress also play essential roles in the progression of cancer (Moneim 2015, Saha, Lee et al. 2017). For instance, an increased oxidative stress is a characteristic in the aging process, and continued oxidative stress can induce chronic inflammation that leads to cancer (Reuter, Gupta et al. 2010). Therefore, the regulation of AAAs has the potential to amplify oxidative stress during the onset and progression of diseases. This is because excess AAA, such as phenylalanine and tryptophan, can induce the production of Reactive Oxygen Species (ROS) by activating the mammalian target of rapamycin (mTOR) and promoting oxygen consumption and mitochondrial metabolism (Saxton and Sabatini 2017, Mossmann, Park et al. 2018) (Wang, Ji et al. 2015). In addition, mechanistic target of rapamycin complex 1 (mTORC1) becomes specifically activated with excess AAA while the AMP-activated protein kinase (AMPK) is inhibited (Chiacchiera and Simone 2009, Thiem, Pierce et al. 2013, Vadlakonda, Dash et al. 2013, Zhao, Hu et al. 2017). Cell growth and metabolism rely on mTORC1 as a critical regulator through the modulation of lipid and protein synthesis, autophagy, and biogenesis (Takahara, Amemiya et al. 2020). Dysregulation of mTORC1 and related enzymes such as AMPK is associated with diseases such as cancer and neurodegenerative disorders (Blommaart, Luiken et al. 1995, Sengupta, Peterson et al. 2010, Saxton and Sabatini 2017, Takahara, Amemiya et al. 2020). AMPK maintains the production and consumption of ATP in eukaryotic cells (Rossi, Redaelli et al. 2018) and is critical for the transcription factors TFEB and TFE3 activity (Hardie

2007). Its inhibition blocks the targeting gene associated with autophagy-lysosome and accounts for the accumulation of lipid species (Figure 1.1). With the failure of autophagy and lipophagy initiation, an accumulation of lipid droplets (LDs) and increase in ROS within cells can perhaps be observed and quantified. Ultimately, these altered metabolic activities can contribute to mitochondrial dysfunctions that lead to the production of malignant precursors from healthy cells (Porporato, Filigheddu et al. 2018). Furthermore, LDs are a distinctive feature of cellular stress and oxidative stress can lead to LD accumulation (Khatchadourian, Bourque et al. 2012, Younce and Kolattukudy 2012, Lee, Zhang et al. 2013). Dysfunctional mitochondria is characteristic of cancer progression (de la Cruz López, Toledo Guzmán et al. 2019), and the upregulation of mTORC1 is implicated in the lipid metabolism of mitochondria. Due to the lack of non-invasive, label-free imaging methods, the role of AAA, specfically phenylalanine and trytophan, in cellular metabolism such as lipid synthesis and protein synthesis is unclear.

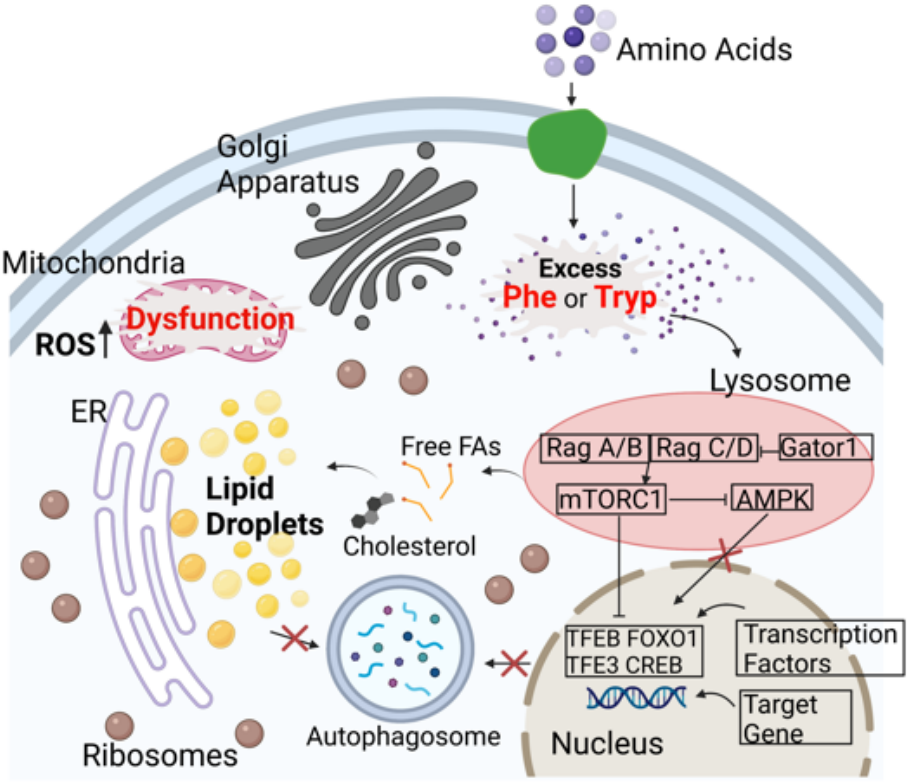

Figure 1.1. Illustration of how excess amino acids upregulate the mTORC1 pathway in cells. mTOR is a key regulator of lipid metabolism. With higher available nutrients, such as Phe (Phenylalanine) and Tryp (Tryptophan), mTORC1 is active and AMPK becomes inactive. mTOR inhibits the transcription factors, that include TFEB and TFE3, to block the targeting of transcriptional genes associated with the autophagy-lysosome (Chiacchiera and Simone 2009, Thiem, Pierce et al. 2013, Vadlakonda, Dash et al. 2013, Zhao, Hu et al. 2017). This ultimately results in lack of autophagy and start of lipophagy leading to an increase in lipid droplet accumulation and ROS. The increase in oxidative stress results in the dysfunction of the mitochondria and ER stress (Zhang, Evans et al. 2018, Paquette, El-Houjeiri et al. 2021, Ralhan, Chang et al. 2021). Abbreviations: (AMPK), mechanistic target of Rapamycin complex 1 (mTORC1), (TFEB), (TFE3)

AAA studies usually rely on gas chromatography (GC) and/or mass spectroscopy (MS)-based imaging techniques to study lipids (Li, Cheng et al. 2021). Electrospray ionization (ESI)-MS has also been used to study how fatty acids quantitively change with AAA supplementation (Ma, Chen et al. 2021); however, these imaging technologies lack the ability to show the lipids' spatial distribution in cells. Other methods, such fluorescence microscopy or magnetic resonance imaging (MRI), require fluorescent dyes or simply have limited spatial resolution. Moreover, the

required dyes for some of these techniques can potentially interfere with molecular activities happening within the cells (Di Gialleonardo, Wilson et al. 2016). On the other hand, matrix-assisted laser desorption/ionization (MALDI) has been made used to study how biomarkers can regulate fatty acid metabolism in cancer cells without affecting native distributions (Pirman, Efuet et al. 2013), but suffers from relatively shallow imaging depths, and poorer spatial resolution despite the additional sample preparation (Murphy, Hankin et al. 2009, Bowman, Bogie et al. 2020). Atomic force microscopy is another powerful technique that can be used to observe lipid formation; however, it is difficult to study the miscibility of multiple lipids (Wang, Shogomori et al. 2012).

Raman spectroscopy and microscopy are relatively new optical techniques that are rapidly outpacing other molecule-specific imaging methods and excels in high resolution and chemical specificity outputs in biological samples (Ghita, Pascut et al. 2012, Daudon 2016, Ember, Hoeve et al. 2017). This study makes use of Deuteriun-Oxide Stimulated Raman Scattering (DO-SRS) for the subcellular analysis of the AAAs regulated metabolic dynamics for molecular signatures including newly synthesized proteins and lipids non-invasively with minimal sample preparations. Heavy water was added to the cell culture media because the deuterium could be enzymatically included into proteins and lipids through de novo biosynthesis. Therefore, metabolic activities can be closely observed using this technique coupled with DO-SRS microscopy (Figure 1.2A). Figure 1.2B displays a typical Raman spectrum that can be obtained by our Raman spectroscopy using D_2O media. Thousands of variables and their multiplexed patterns can be analyzed using a spectral resolution of 1.2 cm^{-1} and a range from 400 cm^{-1} to 3200 cm^{-1}. The Raman peaks that display the strongest patterns, in terms of different intensities and positions, are then selected to be imaged with the DO-SRS microscopy to visualize the spatial distributions of these molecules within the

cell. The output of these techniques is a hyperspectral image (HSI), where an optical focus plane is captured at different Raman shifts. The slice for the HSI displays the areas in which the specific molecular bonds exist, and pixel intensities are directly proportional to these molecular bonds' concentrations (Shi, Zheng et al. 2018). Furthermore, Two Photon Excited Fluorescence (2PEF) microscopy is coupled with DO-SRS to provide additional information of flavin and nicotinamide adenine dinucleotide (NADH) pools in the same region of interest. Flavin and NADH autofluorescence have been associated with redox homeostasis in cells and can imply lipid peroxidation status as well (Mayevsky and Barbiro-Michaely 2009, Surre, Saint-Ruf et al. 2018). Thus, using both DO-SRS and 2PEF methods will allow us to visualize the metabolic dynamics of cells when AAAs are being regulated.

In this study, we utilized DO-SRS microscopy coupled with 2PEF microscopy to observe the metabolic activities of lipids and proteins in cancer cells and investigate the effects of AAA on LD metabolism in HeLa cells. Quantitative lipid turnover rates of different experimental conditions help illuminate how lipid metabolism can be affected with the regulation of phenylalanine and tryptophan. The outcomes support AAAs as targets for the accumulation of LDs and ROS.

1.2 Materials and Methods

1.2.1 Cell Culture

HeLa cells were cultured in Dulbecco's modified Eagles' medium (DMEM), supplemented with 10% fetal bovine serum (FBS) and 1% penicillin/streptomycin (Fisher Scientific, Waltham, MA), and incubated with 5% CO2 at 37°C. After passaging at 80% confluence, cells were seeded at a concentration of 2×10^5/mL onto a 24-well plate. DMEM with 0.5% FBS and 1%

penicillin/streptomycin was used to synchronize the cells for 8 hours. The media was then changed to 50% (v/v) heavy water (D_2O) and treatment media as described below.

For the excess aromatic amino acids condition, phenylalanine and tryptophan were increased as two separate test conditions at a 15x concentration. L-phenylalanine powder (SLCF3873, Sigma Aldrich) and L-tryptophan powder (SLCF2559, Sigma Aldrich) were added to DMEM for the excess groups. Cells were then incubated for 36 hours and fixed on microscope slides afterwards. Next, the cells were gently rinsed with 1x PBS with Calcium and Magnesium ions at 37°C (Fisher Scientific, 14040216), and fixed in 4% methanol-free PFA solution (VWR, 15713-S) for 15 minutes. The cover glass was finally mounted on the cleaned 1mm thick glass microscope slides with 120 μm spacers filled with 1x PBS for imaging and spectroscopy. These samples are stored at 4°C when not in use.

1.2.2 Spontaneous Raman Spectroscopy

A confocal Raman microscope (XploRA PLUS, Horiba) was used to obtain spontaneous Raman spectra. The microscope is equipped with a 532 nm diode laser source and 1800 lines/mm grating. The excitation power is approximately 40mW after passing through a 100x objective lens (MPLN100x, Olympus). The spectrometer collects the intensity values in each region for a range of excitation wavenumbers from 400 cm^{-1} to 3150 cm^{-1}. The acquisition time used for these samples are 90 seconds with a binning of 4, and accumulation of 3 for minimal noise and greater accuracy for the resulting spectra (See Supplemental Figure 1.5A) Each spectrum is taken by targeting the desired subcellular region and an additional spectrum is taken of the background with PBS in the same focal plane. Immediately after, the background spectrum is then subtracted from each subcellular target spectrum.

1.2.3 Stimulated Raman Scattering Microscopy

An upright laser-scanning microscope (DIY multiphoton, Olympus) with a 25x water object (XLPLN, WMP2, 1.05 NA, Olympus) was used for near-IR throughput. Stokes with a wavelength at 1031nm, 6ps pulse width, and 80MHz repetition rate and synchronized pulsed pump beam with a tunable 720-990 nm wavelength, 5-6ps pulse width, and 80 MHz repetition rate were supplied by the picoEmerald system (Applied Physics & Electronics) and coupled into the microscope. A high NA oil condenser (1.4 NA) was used for the collection of the Stokes and pump beams where the sample is mounted. For the water-immersion objective lens, a larger water droplet is placed on the glass cover slip of the sealed sample slide. The Stokes beam is blocked by a high O.D. shortpass filter (950nm, Thorlabs) and transmits the pump beam onto a Si photodiode to detect the stimulated Raman loss signal. A lock-in amplifier at 20MHz is utilized to terminate, filter, and demodulate the output current from the photodiode where the demodulated signal forms the image during the laser scanning as it is processed into the FV3000 software module FV-OSR (Olympus) as shown in Figure 1.2A. The images were collected at 512 x 512 pixels using a dwell time of 80 μs/pixel The images are saved as an OIR graphic file through the acquisition software by the Olympus microscope.

The background image was taken at 1900 cm^{-1} and subtracted from all the SRS images using ImageJ software. For multichannel SRS imaging, the pump wavelength (λ_{pump}) was tuned so that the energy difference between the pump and Stokes beams were matched with the vibrational frequency (Ralhan, Chang et al. 2021).

1.2.4 Two Photon Excitation Microscopy

Label-free autofluorescence of flavins was excited at 800 nm and autofluorescence of NADH was excited at 780nm using the same tunable picosecond laser described in Stimulated Raman Scattering microscopy. Optical-parametric oscillators and amplifiers (OPO and OPA)

sources provide tunable infra-red illumination. This takes place over a broad range of wavelength to allow for simultaneous multi-color imaging (Mahou, Zimmerley et al. 2012). Back scattered emission of flavin and NADH autofluorescence was collected using a 460 nm/515nm filter cube (OCT-ET460/50M32, Olympus). These images were also 512x512 pixels and were acquired with an 8 μs/pixel dwell time using a 150mW power at the laser shutter.

1.2.5 Data Analysis

1.2.5.1 Spectral Analysis

The mathematical modeling operations were conducted using MATLAB. Scripts and functions used for processing the Raman spectra were self-written using built-in functions provided by MATLAB. Origin software was used to display original spectra as shown in Supplemental Figure 1.5A.

The spectral pre-processing consists of several steps that include background removal, baseline correction, and vector normalization. MATLAB software was used to import the raw spectra data. Background was subtracted, and the files were converted into an array where the spectra has been interpolated at every cm^{-1}. The raw data was then graphed for verification, and the baseline correction was performed. The resulting spectra were vector normalized and averaged for each group to reduce the amount of noise on the graph of the biomolecular signals. Each spectral peak is assigned to the vibrations of a particular chemical bond or function group.

1.2.5.2 Image Analysis

Images were processed using MATLAB and ImageJ. To reduce horizontal noise artifacts caused by laser beam scanning, 3D image stacks of lipid droplets underwent bandpass filters and smoothing. Each lipid droplet received a spherical score by calculating the distance between its center of mass and surface. Subsequently, every spherical score of different lipid droplets were

compared with a spherical score of a perfect sphere on the same Euclidean plan. Those lipid droplets with low sphericity scores were discarded. Using ImageJ, ten cell units from three different regions of interest per condition were manually segmented and measured. These cell units were relative in sizes, shapes and randomly selected for analysis.

1.2.5.3 Statistical Analysis

Statistical significance was verified by analysis of variance, checking the mean of more than two groups that are significantly different from each other. The mean and standard deviations were calculated for all the investigated conditions. The data were analyzed using GraphPad Prism for Mac. Significant differences between the controls and treatment groups were compared using the two-way analysis of variance (ANOVA). The data that had p-values lower than 0.05 were identified as statistically significant. MATLAB software was used to process the data for multivariate analysis. Additional statistical analysis was performed on Orange3 Data Mining Tool for greater visualization of the high-dimensional data such as primary component analysis (PCA) for more accurate representation of how the spectrums are compared from the control group to the excess aromatic amino acid groups.

1.3 Results

1.3.1 Raman and DO-SRS Imaging to Identify Changes in Lipid and Protein Synthesis

Metabolic precursors can be tagged with deuterium before getting integrated into newly synthesized lipids and proteins (Miyagi and Kasumov 2016), as shown in Figure 1.2C. DO-SRS enables one to visualize the subcellular spatial distribution of newly synthesized macromolecules with C-D bonds which have a distinguishable Raman peak in the cell silent region at 2150cm^{-1} (Yamakoshi, Dodo et al. 2011, Shi, Shen et al. 2018, Shi, Zheng et al. 2018, Zhang, Shi et al. 2019, Zhao, Chen et al. 2020). 50% D_2O in cell culture media produced distinct C-D Raman bands (See

Supplemental Figure 1.5A). Adding excess essential amino acids to our cell culture media at a 15x concentration introduced differences in the C-D band (Figure 1.2D). Indeed, with LDs being specifically observed, we noticed that both 15x phenylalanine and 15x tryptophan show higher intensities of biomolecules compared to the control group at the 2143 cm^{-1} peak. The lipid turnover rate was visualized with DO-SRS imaging and confirmed with spontaneous Raman spectra by showing that both aromatic amino acids have significant differences between each other and between the control group (See Supplemental Figure 1.6B). Quantitative analysis can aid in understanding the subcellular resolution of LDs by calculating the ratios of the C-D lipid and protein peaks to their respective lipid (2850 cm^{-1}) and protein (2930 cm^{-1}) channels. Ten spectra were measured using Spontaneous Raman spectroscopy. The data was processed using MATLAB to subtract the background and conduct baseline correction. Resulting spectra were then vector normalized and averaged for each group. We observed a significant 7% and 15% increase in the lipid turnover rate between the control and 15x phenylalanine and 15x tryptophan case, respectively. This indicates that excess AAA has the potential to increase LD production. Interestingly, the protein in the C-D region, showed very minimal differences between the control and two experimental conditions (Figure 1.2D). The protein turnover rate, on the other hand, demonstrated an opposite trend to the lipid turnover rate. Specifically, there is a 1.38% decrease in the protein turnover rate between the control and 15x phenylalanine group, and a 6.6% decrease between the control and 15x tryptophan case (Figure 1.2E). However, the C-D protein (2185 cm^{-1}), the protein channel (2930 cm^{-1}), the C-D lipid (2150 cm^{-1}) and the lipid channel (2850 cm^{-1}) are just parts of the Spontaneous Raman spectra. Principal component analysis (PCA) shows that 19 principal components (PCs) account for 98% of the variance in the experimental groups of this study. A t-SNE diagram is used to visualize the top 15 principal components as shown in

Supplemental Figure 1.5B. At least one dimension that distinguishes the effects of AAA on Raman spectra of HeLa cells under different treatments can be observed. This can show that even at 15x increase in concentration, we can still observe some profound differences compared to the control group. Although this verifies that phenylalanine and tryptophan do have a notable effect on lipid metabolism in cancer cells, PCA and t-SNE plots have limited ability to isolate specific peaks that contribute to major variances on Raman spectra in this study.

As various fluctuations of C-D protein and lipid signals were observed from Spontaneous Raman spectra of HeLa LDs, DO-SRS microscopy was used to visualize spatial distribution of C-D signals to a greater depth. A workflow of DO-SRS is displayed in Figure 1.2A. DO-SRS affords the convenience of visualizing lipid and protein metabolism simultaneously (Shi, Zheng et al. 2018). Both the C-D lipid and C-D protein channel were utilized, and the signals were clearly different between the control and the AAA conditions (Figure 1.2F). Image analysis highlights the spatial distribution of the lipids and proteins, and the de novo synthesis of these compounds emphasizes how much the LDs were affected by the excess phenylalanine and tryptophan.

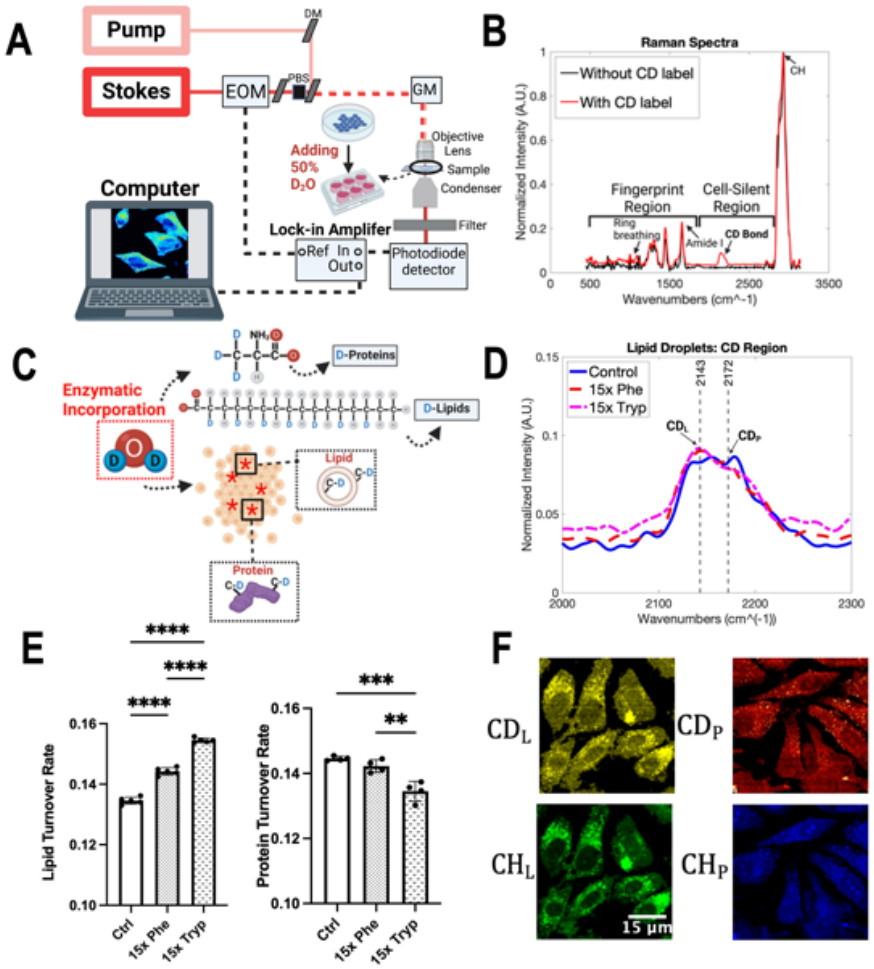

Figure 1.2. DO-SRS microscopy and Spontaneous Raman spectra.
A) Schematic diagram of the experimental setup SRS system workflow (Li, Jiang et al. 2017). Abbreviations: DM (dichroic mirror), EOM (electro-optical modulator), PBS (polarizing beam splitter), GM (galvometer mirror). **B)** Spontaneous Raman spectra without D_2O incorporation (black) and 50% of D_2O addition (red). **C)** Magnification of how HeLa cells were treated with D_2O and excess aromatic amino acids, Phenylalanine (Phe) and Tryptophan (Tryp). Red asterisks represent the effect of D_2O to the cells. **D)** Results from processed Spontaneous Raman spectrums for the control (Ctrl) group (blue), 15x Phenylalanine-treated (15x Phe) group (red), and 15x Tryptophan-treated (15x Tryp) group (magenta) from HeLa cells. Spectrums were taken with the laser focused on structures that resembled lipid droplet organelles under the brightfield imaging system. Each Raman spectrum had a background spectrum from the PBS removed before being normalized, averaged, and baseline corrected. Peaks labeled correspond to Deuterium-labelled lipid (CD_L) and Deuterium-labelled protein (CD_P) (Yamakoshi, Dodo et al. 2011, Shi, Shen et al. 2018, Shi, Zheng et al. 2018, Zhang, Shi et al. 2019, Zhao, Chen et al. 2020), which were observed more specifically to understand how 50% D_2O cell media with the excess aromatic amino acids affected the lipid metabolic activity. **E)** Quantification of the mean Raman results from CD_L and CD_P peaks for HeLa under control and experimental conditions. ****$p<0.0001$, ***$p<0.001$, **$p<0.01$ from 2-way ANOVA test. **F)** DO-SRS images of HeLa cells in C-D lipid (2145 cm^{-1}) and C-D protein (2175 cm^{-1}) on the top row. Bottom row shows SRS images of cells in the protein and lipid channels from 2940 cm^{-1} and 2845 cm^{-1}.

1.3.2 The Effect of Excess AAA on Lipid Metabolic Pathways determined with DO-SRS techniques

DO-SRS imaging of experimental and control groups show differences between LD signals. Using ImageJ, the same amount of cell units from three samples are manually segmented and measured, as indicated by dotted-white borders in Figure 1.3A. With only the control case, there is some signal in the C-D lipid and protein channel; however, the 15x phenylalanine (15x Phe) and 15x tryptophan (15x Tryp) display even stronger signals (Figure 1.3A). The 15x Tryp case shows a profound signal for lipid droplets in the C-D lipid channel but a weaker signal in the C-D protein channel. A similar trend occurs for the 15x Phe as compared to the control case for both lipid and protein channels. Quantitative analysis shows the accumulation of synthesized lipid and protein (Figure 1.3B). Although the statistical analysis did not show significance, the ratiometric results demonstrate that the AAA conditions have greater lipid synthesis by 10-17% but reduced protein synthesis by approximately 10%. Protein synthesis is critical in the study of metabolic dynamics, and although D-labeled amino acids can be used to tack protein synthesis (Li, Jiang et al. 2017), D_2O has proven to be more efficient and consistent (Shi, Zheng et al. 2018). From our results, an increase in AAA can have the potential to increase lipid synthesis but decrease protein synthesis using 50% v/v D_2O in the cell culture media. This evidence infers the possibility of a lack of autophagy taking place in the cells that causes an increase in LDs and promotes the generation of ROS as well as mitochondrial dysfunction (Chiacchiera and Simone 2009, Younce and Kolattukudy 2012, Nguyen, Louie et al. 2017, Zhang, Evans et al. 2018). DO-SRS has proven to be very effective and accurate to track the lipid and protein synthesis of HeLa cells and observing how AAA can show critical changes of the cells' signal.

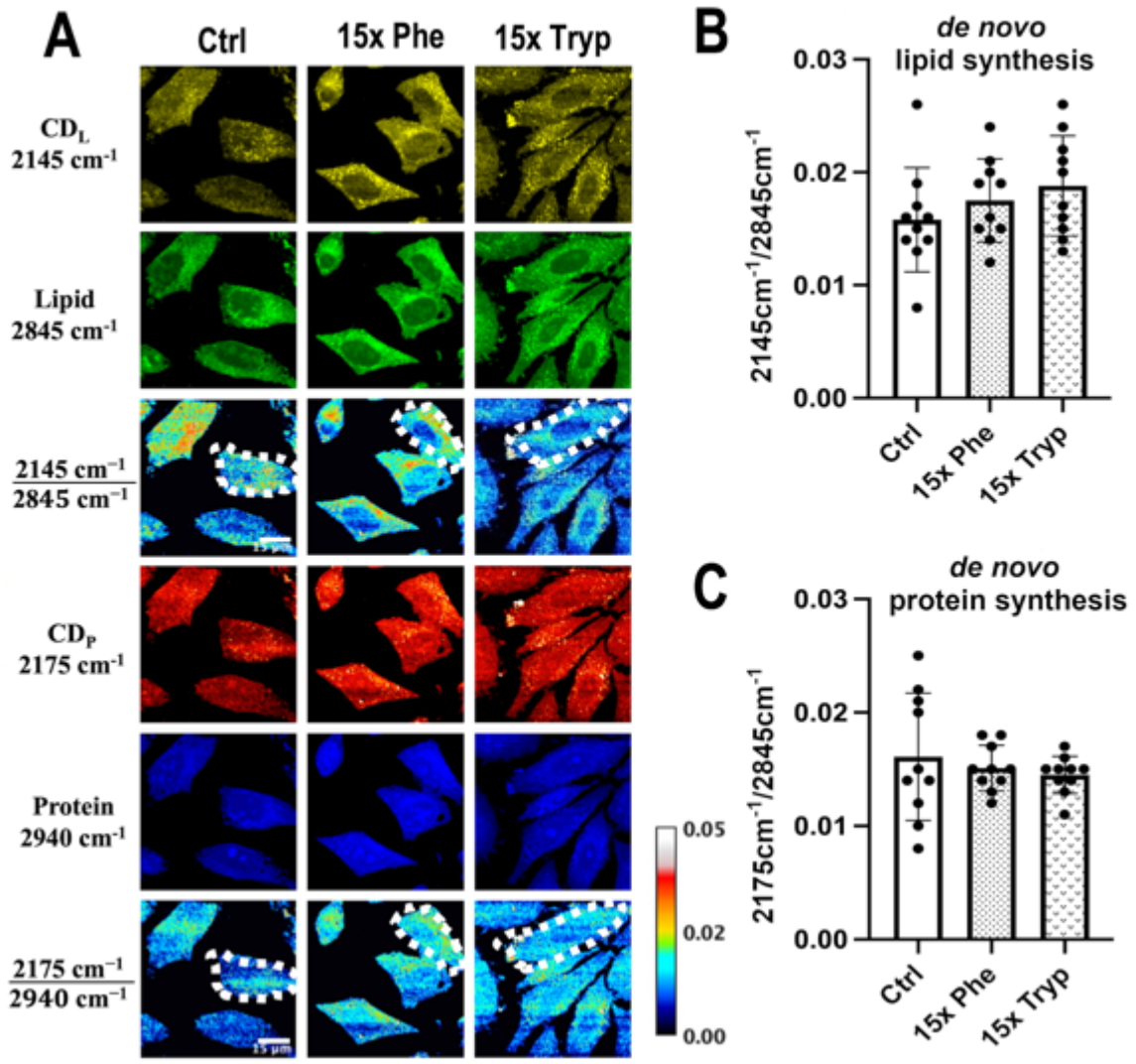

Figure 1.3 DO-SRS microscopy visualizes in vitro protein and lipid metabolism simultaneously in HeLa cells.
A) DO-SRS microscopy visualizes Deuterium-labelled lipid (CD_L; 2145 cm^{-1}), lipid (CH_2; 2845 cm^{-1}), Deuterium-labelled protein (CD_P; 2175 cm^{-1}) and protein (CH_3; 2940 cm^{-1}) channels in in HeLa cells for control (ctrl), 15x phenylalanine (15x phe), and 15x tryptophan (15x tryp). The $2145cm^{-1}/2845cm^{-1}$and $2175cm^{-1}/2940cm^{-1}$ ratios are calculated to understand metabolic activities of HeLa cells between the ctrl, 15x phe and 15x tryptophan 15x tryp groups. Multiple cell units are selected for calculating absolute intensities of $2145cm^{-1}/2845cm^{-1}$ and $2175cm^{-1}/2940cm^{-1}$ ratios between experimental groups. **B-C)** Ratiometric analysis of lipid and protein turnover rates to compare control group with experimental conditions with p-value of 0.1498 and 0.6816 respectively from the 2-way ANOVA test.

Using SRS and 2PEF microscopy, multimodality imaging of unsaturated lipid (~3011 cm^{-1}), saturated lipid (~2880 cm^{-1}) and flavin, NADH signals were acquired (Figure 1.4A). Similarly,

the same amount of cell units from three samples are manually segmented and measured using ImageJ as indicated by the dotted-white borders in Figure 1.4A. Oxygen is a critical metabolite that accepts electrons from reduced NADH and flavin at the end of the electron transport chain (ETC) (van Manen, Lenferink et al. 2008). However, electrons can escape NADH and flavin before reaching the end of the ETC in mitochondria to produce ROS. In some cancer cells, the accumulation of ROS induces the oxidation of polyunsaturated fatty acids, promotion of saturated lipid production, and depletion of NADH levels (Watmough, Bindoff et al. 1990, Wang, Palmfeldt et al. 2019, Zhang and Boppart 2021) in response to the oxidative stress. However, HeLa cells have been shown to increase polyunsaturated lipid levels in response to elevated ROS [60]. Raman shifts have been used to describe the magnitude of unsaturated and saturated lipids at 3011 cm^{-1} and 2880 cm^{-1} (Figure 1.4A), respectively (Da Silva, Bresson et al. 2009, Jamieson, Li et al. 2018).

Ratiometric SRS images demonstrate that excess AAA-treated cells have an elevated ratio of unsaturated lipid/saturated lipid by 10% as compared to the control HeLa cells. However, neither the lipid saturation nor the optical redox ratio was significantly different between the two excess AAA-treated cells (Figure 1.4B). Quantitative analysis further showed statistical significance between the control group and the experimental groups for both the unsaturated lipid to saturated lipid and optical redox ratio, defined as Flavin/(Flavin + NADH) autofluorescence intensity. Moreover, the optical redox ratio demonstrated higher statistical importance between the two experimental groups with a 50% increase in the ratio (Figure 1.4D). The enrichment of NADH and flavin demonstrates an increase in the accumulation of LDs as β-oxidation is hampered (Watmough, Bindoff et al. 1990, Wang, Palmfeldt et al. 2019). Unsaturated lipid images were weaker than the saturated lipid channel which displayed a higher signal to noise ratio. With the

manipulation of AAAs and the consequential changes in lipid content, LD structure, number, and distribution may be affected as well.

In addition to multimodal imaging, SRS has the capability to perform 3-D image reconstruction of LDs in control and AAA-treated HeLa samples. In short, the microscopy produces a set of cross-sectional images throughout the entire depth of a selected region of interest. In this study, we tune the stimulated Raman loss (SRL) to 2845 cm^{-1} and scan a region of interest from the top layer to the bottom layer with a step size of 1 micron (Figure 1.4B-C). Quantitative analyses of LD count and size were performed for each condition (Figure 1.4E). Both excess AAA-treated cells exhibited greater counts of LD but reduced volumetric properties compared to the control cell (Figure 1.4C). Qualitatively, the presence of excess Phe causes clusters of LD on one side of the cell's nucleus, whereas the presence of excess Tryp leads to a uniform distribution of LDs around the cell's nucleus (Figure 1.4B). During the span of this study, we were only able to investigate LD volume and counts of three single cell units per condition. Therefore, the results were not statistically significant, and require further research.

The abnormal accumulation or depletion of LDs are hallmarks and perhaps causes of various human pathologies (Thiam and Beller 2017). LD-coating proteins greatly influence LD's size and counts, ultimately affecting LD accumulation or depletion. For instance, Perilipins are a group of LD-coating with amphipathic helices (AHs) binding domains that target LD surfaces (Thiam and Dugail 2019). Depending on the Perilipin species and their phosphorylated states, the binding of the proteins onto LD surfaces can initiate lipolysis or lipogenesis (Sztalryd and Brasaemle 2017). Previous studies have shown that an increased number of bulky hydrophobic amino acid residues such as Tryp and Phe on the hydrophobic face of AH in these proteins can impair their binding affinity to LDs (Thiam and Dugail 2019). It has been reported that with the

failure of lipolysis from impaired Perilipins, there is an accumulation of numerous small LDs (Schott, Weller et al. 2019). Our 3D volumetric analyses of LDs concur with these previous findings by demonstrating that LDs increase in counts but decrease in volume in the excess AAA groups compared to the control group. Therefore, the presence of excess AAA might impair perilipin function and inhibit lipolysis, which can be visualized *in situ* with high resolution SRS.

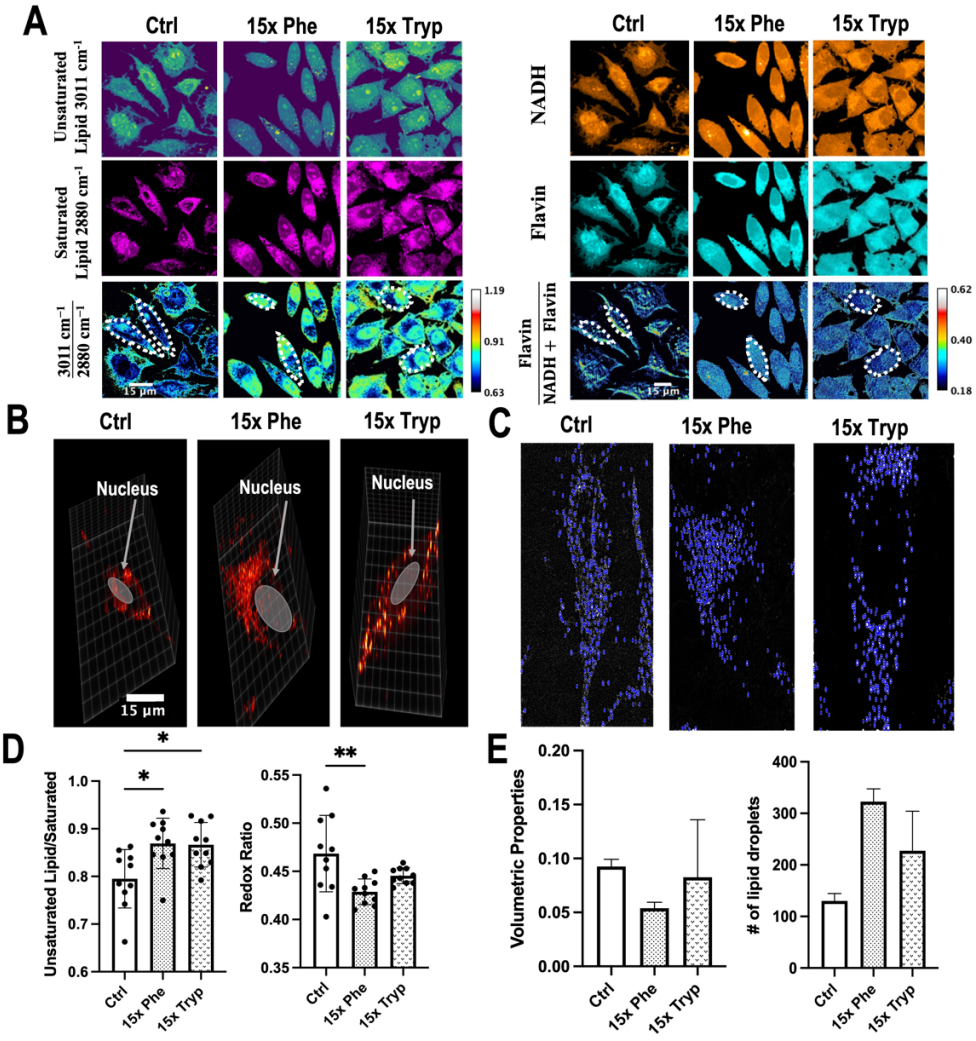

Figure 1.4 Images obtained using label-free SRS and analyzed from the unsaturated fatty acids, saturated fatty acids, NADH, and Flavin channel to observe the autofluorescence between each experimental condition.
A) SRS microscope visualizes in vitro unsaturated fatty acid (3011 cm^{-1}) and saturated fatty acid (2880 cm^{-1}) channels, and 2PEF microscope visualizes in vitro Flavin and NADH channels in HeLa cells for control (ctrl), 15x phenylalanine (15x phe), and 15x tryptophan (15x tryp). Many cell units in the same regions of interest are used for calculating absolute intensities of $3011cm^{-1}$/ $2880cm^{-1}$ and NADH/Flavin. **B)** Single cell maximum intensity projection using SRS image stacks. LDs are highlighted in blue color using a home-made MATLAB script. **C)** The volume and average number of LDs for control and experimental conditions. Excess AAA LDs have a reduced size compared to control group; however, they have a greater number of LDs. **D-E)** Quantifications of $3011cm^{-1}$/ $2880cm^{-1}$ and NADH/Flavin concentration for HeLa cells under control and experimental conditions for given regions of interest. Excess amino acid treated groups shows large statistical significances compared to the control (ctrl) group. ****$p<0.0001$, *$p<0.05$ from 2-way ANOVA test. **D)** SRS microscope visualizes the 3D spatial distribution of lipid droplets on a single cell unit in the control (Ctrl), 15x Phenylalanine (15x Phe) and 15x Tryptophan (15x Tryp) groups.

1.4 Discussion

In this study, we applied DO-SRS and 2PEF microscopies to investigate aromatic amino acids and their effects on redox homeostasis in HeLa cells. Lipid droplets were selected because they can provide critical metabolic insights for diseases such as cancer (Cruz, Barreto et al. 2020) and heavy water was used to track newly synthesized lipid and protein. These carbon-deuterium bonds display distinct signals in the cell silent region on a Raman spectrum, allowing us to quantify and visualize these newly synthesized bonds *in situ*. In addition, 2PEF was used to provide spatial distribution of flavin and NADH at subcellular resolution. Therefore, by using DO-SRS and 2PEF in this study, we can understand metabolic changes of HeLa cells under different excess AAA treatments and advance current diagnostic methods for these diseases with our findings (Moneim 2015, Parthasarathy, Cross et al. 2018).

Lipid, protein, flavin and other biomolecules have been proven to be indicators or metrics to measure progression of diseases (Heikal 2010). With DO-SRS, we were able to visualize and quantify newly synthesized lipids and proteins. We observed increased de novo lipogenesis and a slight decrease in de novo protein synthesis in excess AAA treated groups compared to the control group (Figure 1.3B-C). These changes were supported by our Raman spectra collected by Spontaneous Raman Spectroscopy (See Supplemental Figure 1.5A). Hyperspectral images of unsaturated and saturated lipids were visualized at their respective wavenumbers to understand the effects of oxidative imbalance caused by excess AAA in HeLa cells. The ratios of unsaturated lipid/saturated lipid were calculated and compared across three conditions. The excess AAA-treated groups exhibited increased unsaturated lipid/saturated lipid compared to the control group. 2PEF was used to excite NADH and flavin in HeLa cells. The redox ratios of Flavin/NADH+Flavin were calculated, compared, and related to the ratios of unsaturated

lipid/saturated lipid. Both excess AAA-treated groups exhibited increased redox ratios compared to the control group. Previous studies have showcased that lower optical redox ratios correlated with increased ROS during cancer progression (Alhallak, Rebello et al. 2016). In response to oxidative imbalance, HeLa cells display decreased levels of mono- and di-unsaturated, but increased levels of polyunsaturated lipids (Rysman, Brusselmans et al. 2010, Munir, Lisec et al. 2019). However, this effect varies across different cancer types (Lisec, Jaeger et al. 2019). In our study, both AAA-treated groups had elevated ROS by displaying lower optical redox ratios compared to the control. Because of the elevated ROS, both AAA-treated cells in our study supported previous findings by showcasing increased levels of unsaturated lipids and decreased levels of saturated lipids, ultimately leading to higher unsaturated lipids to saturated lipids ratios in AAA-treated cells compared to the control group.

In addition, 3D reconstruction images of LD were collected by our SRS system to study quantitative features such as counts and volume of LDs. Previous studies have demonstrated that LD-coating protein exhibit reduced binding affinity for LDs in the presence of excess AAA (Thiam and Dugail 2019). Consequently, the failure of LD-coating protein binding can interfere with lipolysis and result in an accumulation of numerous small LDs (Schott, Weller et al. 2019). Our results support these studies by highlighting that both excess AAA groups exhibited lower volumetric properties, but higher counts of LDs compared to the control group. This outcome may infer the failure of binding of LD-coating protein onto LD surfaces and higher ROS synthesis rate (Moneim 2015, Saha, Lee et al. 2017). However, further research to investigate is needed to confirm this finding using optical techniques.

In our study, excess AAA decreased the volume of LDs but increased their counts. Perhaps, this was done by affecting the binding affinity of LD-coating proteins onto LD surfaces and

decreasing lipolysis. However, further investigation of lipid-protein interactions is needed to confirm DO-SRS data. Furthermore, lower optical redox ratios were observed in excess AAA-treated cells, which corrolated to elevated ROS and increased unsaturated lipids to saturated lipids ratios. To guard against oxidative stress and apoptosis induced by ROS, HeLa cells produce more unsaturated lipids than saturated lipids during their progression (Rysman, Brusselmans et al. 2010, Munir, Lisec et al. 2019). Therefore, our study provides a better understanding of imbalanced oxidative stress effects onto HeLa cells under excess AAA treatments and showcases DO-SRS coupled with 2PEF as non-invasive, high-resolution imaging systems to study metabolic activities *in situ*.

1.5 Conclusion

In summary, this study showcases the effects of excess AAAs on cellular metabolic activities of cervical cancer cell lines and how lipid droplet phenotypes can be used as potential indicators in developments of future diagnostic methods for cancer and other closely related diseases. Without the need of labeling dyes that can interfere with normal physiological environments in a cellular sample, the state-of-the-art, non-invasive DO-SRS microscopy and 2PEF microscopy can visualize and quantify metabolic changes of various biomolecules including protein, lipid, flavin, NADH. In addition, Deuterium Oxide (D_2O) allows us to locate these molecules *in situ* using C-D signals in the cell silent region with DO-SRS. In addition to phenylalanine and tryptophan, a water-insoluble tyrosine aromatic amino acid is not included in this study (Bowden, Sanders et al. 2018). However, we intend to investigate the effects of tyrosine to obtain a holistic understanding of AAA on cellular metabolic activities in cancer and other closely related diseases. A non-linear optical second-harmonic generation (SHG) can also be applied to our SRS system to study collagen and their structure under the influence of AAA in

HeLa xenograft models. Overall, our study demonstrates the useful applications of optical techniques such as DO-SRS and 2PEF in visualizing metabolic changes *in situ* with high resolution. Eventually, these methods can be translated to clinical settings to improve current diagnostic tools for diseases such as cancer and neurodegeneration.

1.6 Supplemental Figures

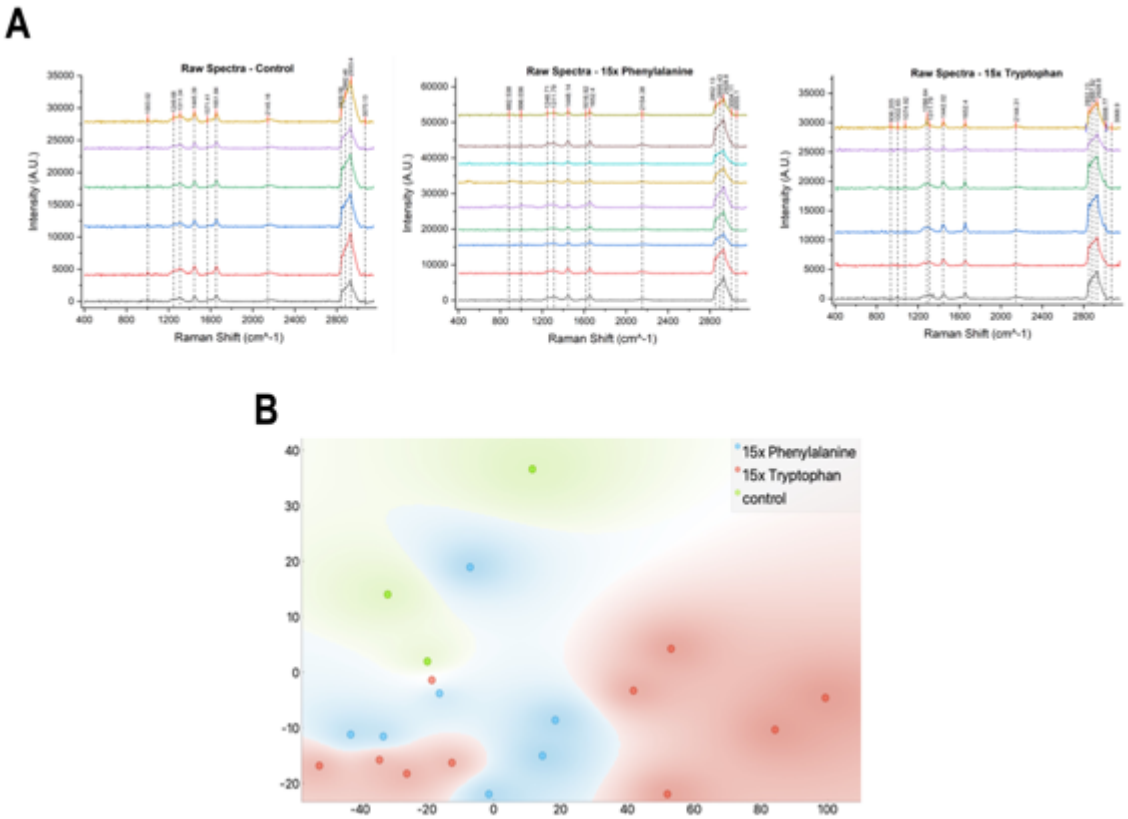

Figure 1.4 Spectra obtained from Spontaneous Raman spectroscopy using 90 second acquisition time and accumulation of 3. Analysis of Spontaneous Raman spectroscopy results from HeLa cells.
A) Results obtained from control and experimental conditions: 15x Phenylalanine and 15x Tryptophan. **B)** t-SNE distributions between control treated samples and excess AAA treated samples.

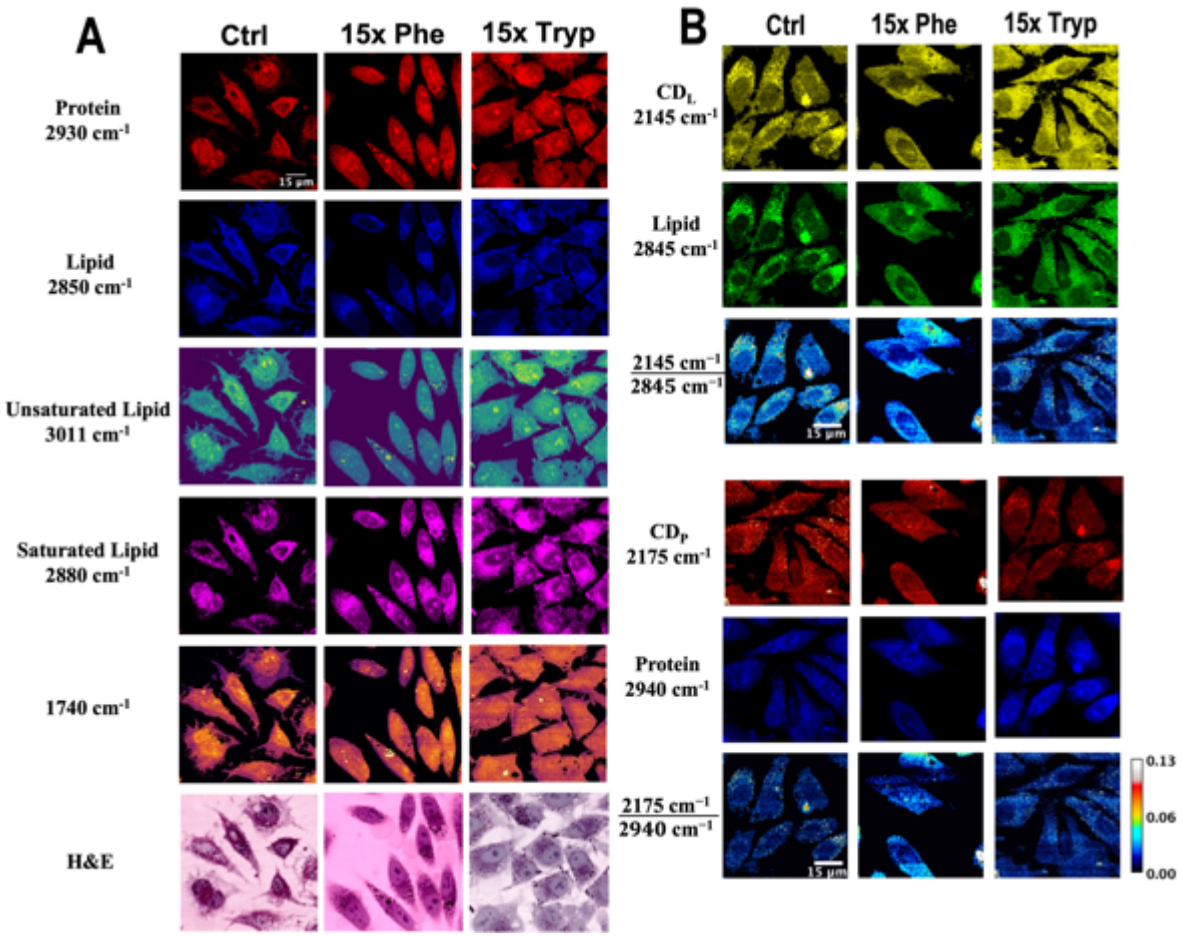

Figure 1.5 Multiplexed imaging of HeLa cells between control (ctrl), 15x Phenylalanine (15x Phe), and 15x Tryptophan (15x Tryp) using label-free SRS and DO-SRS imaging systems. **A)** Multiplexed images of ctrl, 15x Phe, and 15x Tryp of protein (CH_3; 2940 cm^{-1}), lipid (CH_2; 2845 cm^{-1}), unsaturated lipid (3011 cm^{-1}), saturated lipid (2880 cm^{-1}) and 1740 cm^{-1} channels. Hematoxylin and Eosin staining images are produced by combining the protein and lipid channels using FIJI. **B)** DO-SRS images of Deuterium-labelled lipid (CD_L; 2145 cm^{-1}), lipid (CH_2; 2845 cm^{-1}), Deuterium-labelled protein (CD_P; 2175 cm^{-1}) and protein (CH_3; 2940 cm^{-1}) channels of HeLa cells in different groups.

Chapter 1, in full, is a reprint of the material as it appears in Visualizing Cancer Cell Metabolic Dynamics Regulated with Aromatic Amino Acids Using DO-SRS and 2PEF Microscopy 2021. Bagheri, P., Hoang, K., Fung, A.A, Hussain, S., & Shi, L. Frontiers in Molecular Biosciences, 8, 779702. https://doi.org/10.3389/fmolb.2021.779702. The thesis author was the primary investigator and author of this paper.

CHAPTER 2. SUBCELLULAR IMAGING CANCER METABOLIC ACTIVITIES UNDER SERINE REGULATION USING DO-SRS MICROSCOPY

Abstract: Lipid and protein metabolism have been implied to be major metabolic pathways that take part in cancer diseases. The synthesis of proteins and lipids have become a necessity for cell survival, growth, and proliferation. Optical imaging techniques that are high resolution present a dynamic application to understand how lipids and proteins are affected in cancer metabolism. In this study, we utilized D_2O (heavy water)-probed stimulated Raman scattering microscopy (DO-SRS) to directly visualize the metabolic dynamics of cancer cells under the regulation of the non-essential amino acid serine in culture media. The cellular spatial distribution of newly synthesized lipids and proteins were observed and quantified in this experiment. Raman spectra showed excess serine increases both lipid and protein synthesis in HeLa cells while lack of serine will inhibit cell growth. DO-SRS imaging verified that cells with 10x and 20x added serine concentration will have a significant upregulation of *de novo* protein synthesis and lipogenesis whereas cells with only 0.25x serine have a notable decrease in both lipid and protein turnover rate. Furthermore, we found an accumulation of saturated and unsaturated lipids in excess serine cells, suggesting that these specific lipids play an imperative role in cell survival. We also detected rise in Cytochrome c with a surplus of serine but an opposite effect when depriving cells from serine, suggesting that this protein contributes to the promotion of cancer disease. Our study demonstrates how regulation of serine is impactful for cancer cell metabolism by using new imaging platforms such as DO-SRS.

2.1 Introduction

Metabolic pathways that are used to produce macromolecules for required cell survival and growth especially in cancer diseases have become common topics in research (Yang and Vousden

2016). Accumulating evidence has indicated that exogenous supply of amino acids is required for highly proliferative cancer cells (Phillips, Sheaff et al. 2013, Yang and Vousden 2016). This is simply because rapidly growing cells demand a high amount of each amino acid, and *de novo* synthesis pathways may not supply enough for each cell. In addition, with cancer diseases, there are changes and mutations in various enzymes needed to synthesize particular amino acids which can therefore hinder *de novo* synthesis (Hennequart, Labuschagne et al. 2021, Zhao, Fu et al. 2021). Cancer cells become very dependent on specific amino acids one of which is the non-essential amino acid serine. Previous studies have suggested that the lack of exogenous serine will inhibit the growth of cancer cells *in vitro* and *in vivo*; however, excess serine may drive tumorigenesis forward (Kalhan and Hanson 2012, Gao, Lee et al. 2018, Sullivan, Mattaini et al. 2019, Muthusamy, Cordes et al. 2020, Hennequart, Labuschagne et al. 2021). As seen in Figure 2.1, adding a surplus of serine to culture media can activate the mechanistic target of rapamycin complex (mTORC1) because heterodimers of the recombination-activating genes (Rag) small guanosine triphosphate (Rag A/B and Rag C/D) are initiated, inducing the ras homolog enriched in brain (RHEB) G-protein which plays an imperative role for starting mTORC1 (Sancak, Bar-Peled et al. 2010, Saxton and Sabatini 2017, Yang, Jiang et al. 2017). Thus, AMP-activated protein kinase (AMPK) and 4E-binding protein 1 (4E-BP1) are inhibited while S6 kinase beta-1 (S6K1) is upregulated (Chiacchiera and Simone 2009, Vadlakonda, Dash et al. 2013, Ghosh and Kapur 2017, Zhao, Hu et al. 2017, Woodcock, Eley et al. 2020). This leads to lack of autophagy and an increase in lipid and protein synthesis ultimately leading to cancer cell survival and growth (Takahara, Amemiya et al. 2020) (Figure 2.1). The changes in these metabolic activities can promote more oxidative stress and mitochondrial dysfunctions that produce infectious precursors from healthy cells (Saxton and Sabatini 2017, Takahara, Amemiya et al. 2020). Upregulation of

mTORC1 is involved in the lipid and protein metabolism of the mitochondria as this defective organelle contributes to cancer proliferation (Younce and Kolattukudy 2012, Lee, Zhang et al. 2013, Porporato, Filigheddu et al. 2018, de la Cruz López, Toledo Guzmán et al. 2019). With the need of non-invasive and label-free imaging techniques, it remains unclear how serine affects the lipid and protein metabolism in cancer cells.

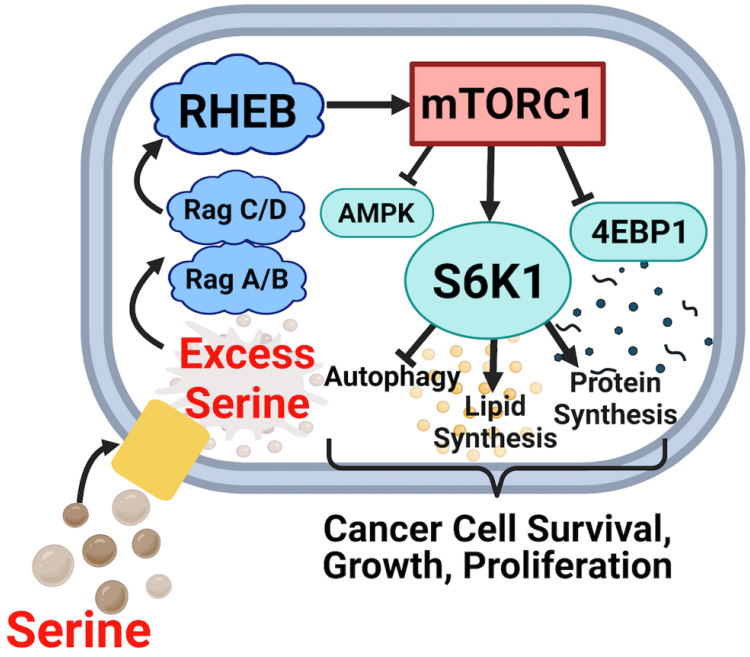

Figure 2.1 Illustration of how excess serine upregulates the mTORC1 pathway in cancer cells. mTOR is a critical regulator for lipid metabolism (Caron, Richard et al. 2015, Bagheri, Hoang et al. 2021). With a surplus of nutrients, such as the amino acid serine, heterodimers of the Rag small GTPases (Rag A/B and Rag C/D) become activated, inducing the RHEB G-protein (Sancak, Bar-Peled et al. 2010, Saxton and Sabatini 2017, Yang, Jiang et al. 2017). RHEB plays a critical role in the activation of mTORC1. With the activation of mTORC1, 4EBP1 protein, which impedes protein synthesis, is inhibited and AMPK becomes inactive, and S6K1 protein is induced which regulates multiple cellular functions such as lipid and protein synthesis. (Chiacchiera and Simone 2009, Vadlakonda, Dash et al. 2013, Ghosh and Kapur 2017, Zhao, Hu et al. 2017, Woodcock, Eley et al. 2020). In addition, with the upregulation of S6K1, autophagy becomes inhibited (Takahara, Amemiya et al. 2020). The increase in lipid synthesis causes accumulation of lipid droplets, and rise in protein synthesis induces greater cell survival, growth, and proliferation. Therefore, tumors will develop and continue to spread. Abbreviations: mechanistic target of Rapamycin complex 1 (mTORC1), recombination-activating genes (Rag), guanosine triphosphate (GTP), ras homolog enriched in brain (RHEB), S6 kinase beta-1 (S6K1), 4E-binding protein 1 (4E-BP1), AMP-activated protein kinase (AMPK).

Typical imaging and analytical methods are useful but still limited in many ways. For instance, mass spectrometry (MS)-based techniques or matrix-assisted laser desorption/ionization (MALDI) have low spatial resolution to show lipids in cells (Murphy, Hankin et al. 2009, Pirman, Efuet et al. 2013, Bowman, Bogie et al. 2020, Li, Cheng et al. 2021). Magnetic resonance imaging (MRI) or fluorescence microscopy usually need fluorescent dyes which can interfere with the molecular activities taking place in the cells, and they have limited spatial resolution as well (Di Gialleonardo, Wilson et al. 2016).

More recently, Raman spectroscopy has been used as a nondestructive technique as it is based on the vibrating molecules that induce an inelastic scattering of light (Ghita, Pascut et al. 2012, Ember, Hoeve et al. 2017). A Raman spectrum consists of various chemical bonds vibrating at distinct frequencies which produces different fingerprints from the molecules (Ghita, Pascut et al. 2012, Daudon 2016, Ember, Hoeve et al. 2017). The peaks of a Raman spectrum each corelate to a specific vibrational mode of a chemical bond. Quantitative imaging is created by the Raman scattering signal intensity as it corresponds to the molecular chemical bond concentration. However, spontaneous Raman spectroscopy restricts the imaging speed due to the delicate signal intensity making it difficult to observe the cell's metabolic dynamics. Stimulated Raman scattering (SRS) and Deuterium-Oxide-probed SRS (DO-SRS) is a non-invasive approach that requires minimal sample preparations and can be applied for the subcellular analysis of molecular signatures such as newly synthesized lipids and proteins (Shi, Zheng et al. 2018, Bagheri, Hoang et al. 2021, Li, Zhang et al. 2021, Li, Bagheri et al. 2022). The imaging speed for this technique is notably faster by about 1000 times compared to spontaneous Raman. The high level of sensitivity is superior in its ability for high chemical specificity and subcellular resolution in addition to multiplex imaging. Heavy water (D_2O) is applied as a Raman probe to track the incorporation of

D_2O-derived deuterium labeled macromolecules, identifying the cell's metabolic activities (Berry, Mader et al. 2015, Li, Bagheri et al. 2022). Moreover, D_2O diffuses freely across the cells where deuterium will be integrated with carbon atoms to create C-D bonds in newly formed biomolecules which establishes a peak in the 1800-2800 cm^{-1} region of a Raman spectrum (Figure 2.2A) (Yamakoshi, Dodo et al. 2011, Shi, Shen et al. 2018, Shi, Zheng et al. 2018, Zhang, Shi et al. 2019, Zhao, Chen et al. 2020, Bagheri, Hoang et al. 2021, Li, Zhang et al. 2021, Li, Bagheri et al. 2022). Applying DO-SRS imaging, we can directly observe the cell's metabolic dynamics of lipids and proteins.

In this chapter, we incorporated D_2O to observe the newly synthesized lipids and proteins in HeLa cells with added and deprived exogenous serine from the spontaneous Raman spectra and used DO-SRS microscopy to track the cells' metabolic dynamics *in situ*. Furthermore, we compared lipid subtypes and specific proteins to reveal the metabolic changes in these cancer cells as serine was being regulated. Image analysis and quantifications demonstrated the lipid and protein spatial distributions and how these compounds were influenced by the manipulation of serine concentration.

2.2 Materials and Methods

2.2.1 Cell Culture

HeLa cells were cultured in Dulbecco's modified Eagles' medium (DMEM), supplemented with 10% fetal bovine serum (FBS) and 1% penicillin/streptomycin (Fisher Scientific, Waltham, MA), and incubated with 5% CO_2 at 37°C. After passaging at 80% confluence, cells were seeded at a concentration of 2×10^5/mL onto a 24-well plate. DMEM with 0.5% FBS and 1% penicillin/streptomycin was used to synchronize the cells for 8 hours. The media was then changed to 50% (v/v) heavy water (D_2O) and treatment media as described below.

For the increased amino acid condition, serine was increased at 10x and 20x concentration. L-serine powder (SLCJ6883, Sigma Aldrich) was added to DMEM for the excess groups supplemented with 5% FBS and 1% penicillin/streptomycin (Fisher Scientific, Waltham, MA). For the 0.25x serine case, cells were cultured in media reconstituted from glucose and amino acid free media (D9800-27, US Biological Life Sciences) supplemented with amino acids at appropriate concentrations from a 100x stock solution of amino acids with only 0.25x concentration of serine added. Amino acids were supplemented from a 100x stock solution made separately according to the experiment and the media was supplemented with 50% heavy water, 5% FBS, and 1% penicillin/streptomycin (Fisher Scientific, Waltham, MA). Cells were then incubated for 36 hours and fixed on microscope slides afterwards. When fixing the cells on the microscope slide, the cells were first gently rinsed with 1x PBS with Calcium and Magnesium ions at 37°C (Fisher Scientific, 14040216), and then fixed in 4% methanol-free PFA solution (VWR, 15713-S) for 15 minutes. The cover glass was finally mounted on the cleaned 1mm thick glass microscope slides with 120 μm spacers filled with 1x PBS for imaging and spectroscopy. These samples are stored at 4°C when not in use.

2.2.2 Spontaneous Raman Spectroscopy

Spontaneous Raman spectra of cell samples were measured by a Raman spectrometer that was connected to a confocal Raman microscope (XploRA PLUS, Horiba). A 532 nm diode line focus laser and 1800 lines/mm grating are equipped to the microscope. The laser is focused on the cells using a 100x objective lens (MPLNx100, Olympus) with an excitation power of approximately 40mW. Spectra were collected at 90 second acquisition time with an accumulation of 3 for the greatest accuracy and least noise and measured at the intensity values in each region for a range of excitation wavenumbers from 400 cm^{-1} to 3150 cm^{-1}. Each individual spectrum is

taken by targeting the desired subcellular region and an additional spectrum is taken of the background with PBS in the same focal plane. Peaks were normalized to 1900 cm^{-1} peak, and baseline correction was performed using Origin Lab software and MATLAB. The instrument is calibrated using a silicon line at 520 cm^{-1}.

2.2.3 Stimulated Raman Scattering Microscopy

An upright laser-scanning microscope (DIY multiphoton, Olympus) with a 25x water object (XLPLN, WMP2, 1.05 NA, Olympus) was used for near-IR throughput. Stokes with a wavelength at 1031 nm, 6 ps pulse width, and 80 MHz repetition rate and synchronized pulsed pump beam with a tunable 720-990 nm wavelength, 5-6 ps pulse width, and 80 MHz repetition rate were supplied by the picoEmerald system (Applied Physics & Electronics) and coupled into the microscope. A high NA oil condenser (1.4 NA) was used for the collection of the Stokes and pump beams where the sample is mounted. For the water-immersion objective lens, a larger water droplet is placed on the glass cover slip of the sealed sample slide. The Stokes beam is blocked by a high O.D. shortpass filter (950 nm, Thorlabs) and transmits the pump beam onto a Si photodiode to detect the stimulated Raman loss signal. A lock-in amplifier at 20 MHz is utilized to terminate, filter, and demodulate the output current from the photodiode where the demodulated signal forms the image during the laser scanning as it is processed into the FV3000 software module FV-OSR (Olympus). The images were collected at 512 x 512 pixels using a dwell time of 80 μs/pixel. The images are saved as an OIR graphic file through the acquisition software by the Olympus microscope.

The background image was taken at 1900 cm^{-1} and subtracted from all the SRS images using ImageJ software. For multichannel SRS imaging, the pump wavelength (λ_{pump}) was tuned

so that the energy difference between the pump and Stokes beams were matched with the vibrational frequency (Ralhan, Chang et al. 2021) .

2.2.4 Data Analysis

The mathematical modeling operations were conducted using Origin, MATLAB, and ImageJ software. Scripts and functions used for processing the Raman spectra were self-written using built-in functions provided by MATLAB.

The spectral pre-processing consists of several steps that include background removal, baseline correction, and vector normalization. Origin Lab and MATLAB software were utilized to import the raw spectra data. Background was subtracted, and the files were converted into an array where the spectra has been interpolated at every cm^{-1}. The raw data was then graphed for verification, and the baseline correction was performed. The resulting spectra were vector normalized and averaged for each group to reduce the amount of noise on the graph of the biomolecular signals. Each spectral peak is assigned to the vibrations of a particular chemical bond or function group.

Statistical significance was verified by analysis of variance, checking the mean of more than two groups that are significantly different from each other. The mean and standard deviations were calculated for all the investigated conditions. The data were analyzed using GraphPad Prism for Mac. Significant differences between the controls and treatment groups were compared using the two-way analysis of variance (ANOVA). The data that had p-values lower than 0.05 were identified as statistically significant. MATLAB software was used to process the data for multivariate analysis.

2.3 Results

2.3.1 DO-SRS Imaging of Newly Synthesized Lipids in Cancer Cells Regulated with Serine

To examine the effects of serine in cancer cells, we observed how lipid metabolism was influenced. Excess serine at 10x and 20x concentration was added to the growth media supplemented with 50% D_2O. In addition, another cell group was deprived of serine by adding only 0.25x serine to serine-free growth media. Newly synthesized proteins and lipids can be tagged with metabolic precursors, which in this case we use deuterium as shown in Figure 2.2A. 50% D_2O in cell culture media results in a distinct C-D Raman band in the "cell-silent" region from 1800-2800 cm^{-1} (Figure 2.2B). With different serine concentrations in cell culture media, the C-D band showed differences between the control (1x serine) and each condition (Figure 2.2B). We obtained the spontaneous Raman spectra by focusing on lipid droplets specifically and observed that excess serine produced higher intensity signals at the C-D lipid and protein peaks at 2145 cm^{-1} and 2175 cm^{-1}, respectively. Moreover, excess serine conditions had greater amounts of total lipids within their cells based on the CH stretching region peak at 2850 cm^{-1} (See Supplemental Figure 2.5A), which is consistent with our previous experiment on the incorporation of excess aromatic amino acids (Bagheri, Hoang et al. 2021). For quantification, we used CD/CH as a ratiometric indicator to evaluate the amount of newly synthesized macromolecules that are normalized against any differences within the same cell sample (Figure 2.5B). There is a clear discrepancy in the CD lipid and protein turnover rates between the control and different serine concentrations for the spontaneous spectra. Depriving serine from cancer cells demonstrated reduced lipids and proteins compared to control by approximately 7% and 10%, respectively. Since these molecular bonds are present in our spectra, we used SRS imaging techniques to observe the cell morphology and changes for each condition to further understand the changes in lipid metabolism.

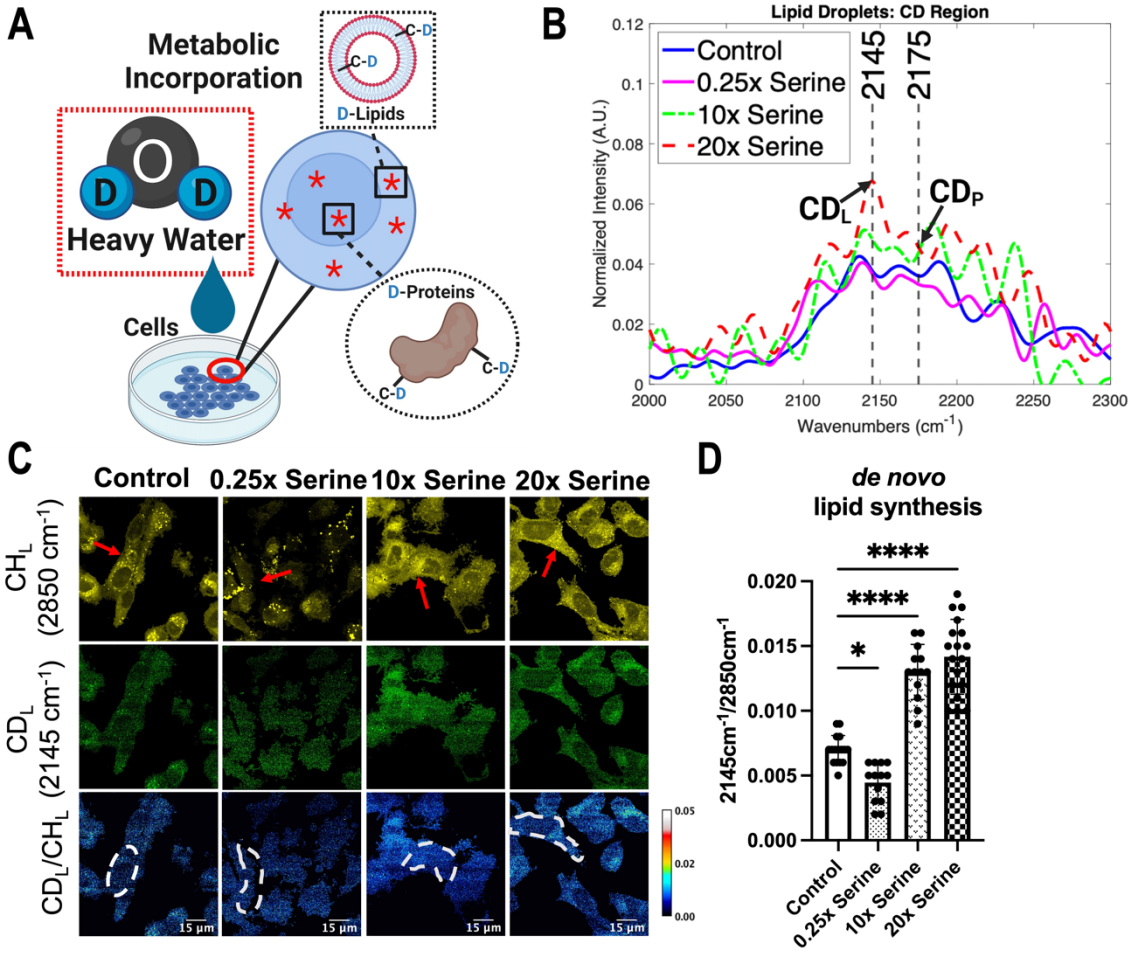

Figure 2.2 Heavy water labeling reveals newly synthesized lipids.
A) Schematic diagram of deuterium oxide probing: Heavy water (D_2O) is metabolically incorporated into cellular lipids and proteins when being added into cell culture media. 50% D_2O is used for this experiment. **B)** Magnification of processed Spontaneous Raman spectra, specifically in the cell-silent region, when HeLa cells were treated with 50% D_2O and regulated with serine at 0.25x, 10x, and 20x concentration. Spectrums were taken with the laser being focused on structures that correspond to lipid droplet organelles which were observed under a brightfield imaging system. Background spectrum from PBS was taken for each lipid droplet Raman spectrum which was subtracted before being normalized to 1900 cm^{-1}, averaged, and baseline corrected. Deuterium-labelled lipid (CD_L) and Deuterium-labelled protein (CD_P) are the following peaks that are labelled, and these were observed more particularly to understand how changes in serine concentration and 50% D_2O affect the lipid metabolism. **C)** Top row displays SRS images of HeLa cells taken at the total lipid channel: 2850 cm^{-1}. The white arrows point towards the lipid droplet organelles. The middle row presents the DO-SRS images at the 2145 cm^{-1} channel, representing newly synthesized (CD) lipids. The bottom row shows the ratiometric images of CD_L/CH_L which were generated to present the location of newly synthesized lipids. Cell units are selected, as outlined in white, to calculate the absolute intensity ratio between the control and experimental groups. **D)** Ratiometric analysis is performed to quantify the lipid turnover rate. 2-way ANOVA test is used to obtain p-values between each condition, ****$p<0.0001$ and *$p<0.05$.

With the incorporation of D_2O in culture media, DO-SRS was used to observe the newly synthesized lipids in HeLa cells (Figure 2.2C). Cells with 0.25x serine showed very little signal intensity and very dispersed lipid droplets compared to control and other experimental conditions. This could potentially be due to the inhibition of mTORC1 and activation of AMPK, so there is an increase in lipid oxidation thereby decreasing overall lipid content and promoting lipid droplet dispersion (Herms, Bosch et al. 2015, Tomar, Jana et al. 2019). Additionally, 0.25x serine caused cells to be relatively smaller in size and not as elongated as the control cells which can be due to the inhibition of cell growth and tumor survival (Polet, Corbet et al. 2016). Quantification confirmed that deprived serine cells have reduced newly synthesized lipids compare to the control by approximately 20% (Figure 2.2D). Previous studies have concluded that the trigger of AMPK can induce fatty acid oxidation and lipid droplet separation; however, we are able to confirm via DO-SRS that lipids are no longer being newly synthesized and cell growth is clearly being slowed down resulting in the impediment of cancer growth (Jones, Plas et al. 2005, Marcinkiewicz, Gauthier et al. 2006, Geeraert, Ratier et al. 2010, Herms, Bosch et al. 2015). Indeed, with AMPK being present, autophagy is also stimulated which can aid in the suppression of cancer-cell survival and induce cell death (Yun and Lee 2018).

On the other hand, 10x and 20x serine concentrated cells showed extremely significant differences in newly synthesized lipids compared to the control cells (Figure 2.2C, D). Both experimental groups showed lipid droplets being clustered around the nucleus of the cell as pointed by the red arrows in Figure 2.2C. The C-D lipid channel also displayed a higher intensity in the 10x and 20x serine cells, and the quantifications confirmed an approximate 60% increase in the excess serine conditions compared to the control (Figure 2.2D). Cells were generally more enlarged and near each other unlike the control and deprived serine groups. The increase in lipid

molecules and cell size can be inferred by the activation of mTORC1 as this trigger will cause lipid synthesis therefore leading to cancer cell growth survival and proliferation (Figure 2.1) (Fingar, Salama et al. 2002, Caron, Richard et al. 2015, Guridi, Kupr et al. 2016, Nguyen, Louie et al. 2017).

2.3.2 Label-Free SRS Imaging of Lipid Subtype Distribution *in vitro*

SRS microscopy has the ability for molecular specificity and subcellular resolution images; thus, we were able to distinguish between distinct spatial patterns of various lipid subtypes. It has been suggested that 2880 cm^{-1}/2850 cm^{-1} ratio is a measurement for lipid lateral packing and conformational state (Choe, Lademann et al. 2016, Uematsu and Shimizu 2021, Li, Bagheri et al. 2022). The close-packed arrangement of lipids is correlated with high values of this ratio which associates with high saturated lipid content (Matthews, Jirasek et al. 2010, Uematsu and Shimizu 2021, Li, Bagheri et al. 2022). In contrast, the level of unsaturated lipid to total lipids in cells identifies with the ratio of 3010 cm^{-1}/2850 cm^{-1} (Jamieson, Li et al. 2018, Bagheri, Hoang et al. 2021). We utilized the label-free SRS imaging features at channels 2850 cm^{-1}, 2880 cm^{-1}, and 3010 cm^{-1}, allowing us to observe the differentiation in lipid subtypes with variations in serine concentrations. Ratiometric images were produced to understand how saturated and unsaturated lipids are distributed at 0.25x, 1x (control), 10x, and 20x serine in HeLa cells.

The output displayed lipids being mainly confined with excess serine presented in cells (Figure 2.3A). SRS signal was very minimal in deprived serine cells, showing only the cell structure, proposing that macromolecular compositions are different for this cell condition compared to the control and excess serine groups. When a normal amount of serine is present as shown in the control case, their signal is higher, and lipids are present demonstrating that serine has a chemical and structural impact on HeLa cells. SRS ratiometric images demonstrated higher

saturated lipid content in 10x and 20x serine conditions unlike 0.25x serine cells which was largely reduced. Lipid droplets are clustered near the nucleus of the cells in excess serine cases indicating that the cells are under oxidative stress, so these organelles are being synthesized to protect the cell from further stress (Jarc and Petan 2019). Quantification of the ratiometric images showed significant increase between control and 20x excess serine cells by approximately 60%, and a large reduction between the 0.25x serine cells by 75% (Figure 2.3B). Previous studies have suggested that when cells become exposed to oxidative stress, lipid droplets tend to accumulate to protect the cell membranes from any peroxidation reactions (Bailey, Koster et al. 2015, Ackerman, Tumanov et al. 2018, Jarc and Petan 2019). This is to control the organelle homeostasis and membrane saturation to enable a longer supply of lipids for cell survival and energy production (Bailey, Koster et al. 2015, Jarc and Petan 2019). In our SRS images and quantifications, we observed a surplus of lipids clustered around the cell when subjected to excess serine, so these lipid droplets could be protecting the cell to promote proliferation and tumor progression.

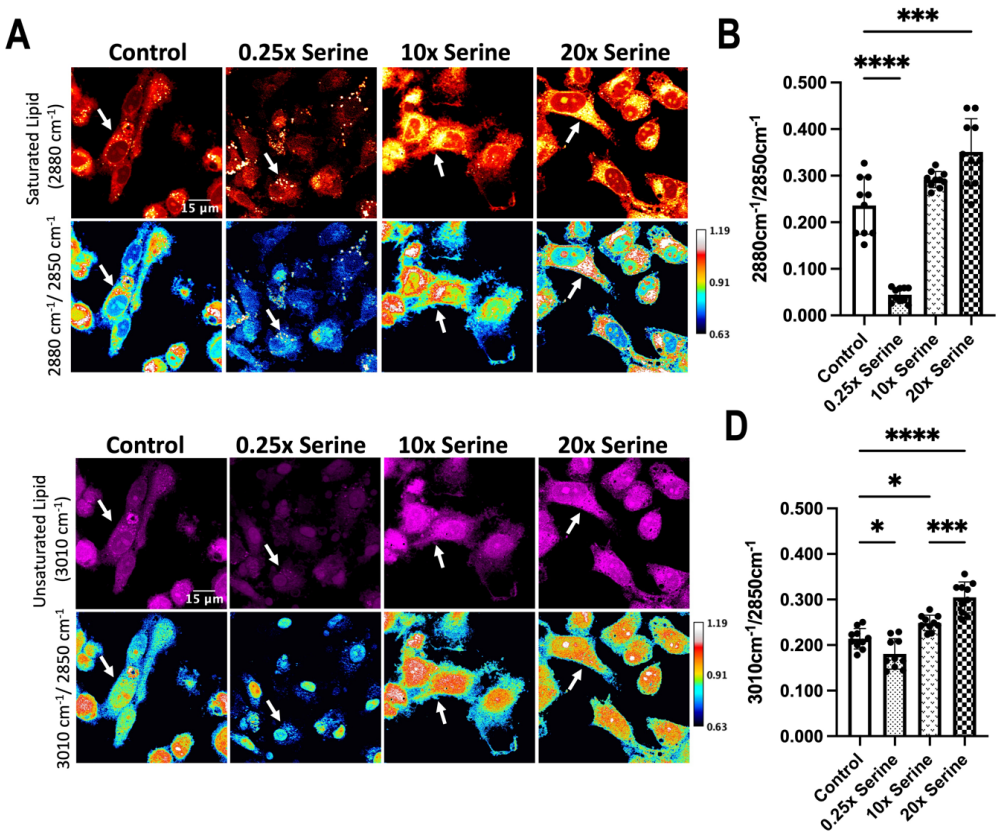

Figure 2.3 Images obtained using SRS microscopy from saturated and unsaturated fatty acids to observe the lipid subtype changes in serine regulated cancer cells with statistical quantifications. **A)** SRS images at 2880 cm^{-1} of control, 0.25x serine, 10x serine, and 20x serine concentrated cells. The ratiometric images of 2880 cm^{-1}/2850 cm^{-1} were processed to show the saturated lipids' distribution and concentration throughout each individual cell unit. The images showed higher saturated lipids with 10x and 20x serine compared to the control condition. 0.25x serine cells displayed much lower saturated lipids throughout. In contrast, excess serine showed the lipids to congregate near the nucleus of the cells, whereas the control group showed saturated lipids dispersed around the cell very discretely. Depriving serine from the cancer cells resulted in very minimal saturated lipids, and they were not uniformly dispersed compared to other experimental groups. The distribution of saturated lipids is consistent in repeated experiments for all control and serine conditions. **B)** Quantification of saturated lipid (2880 cm^{-1}) to total lipid (2850 cm^{-1}) for HeLa cells showed significant differences. ****p<0.0001 and ***p<0.001 from 2-way ANOVA test. **C)** SRS images at 3010 cm^{-1} of control, 0.25x serine, 10x serine, and 20x serine concentrated cells. The ratiometric images of 3010 cm-1/2850cm^{-1} were processed to evaluate the unsaturated lipids' distribution and concentration throughout each cancer cell unit. Unsaturated lipids were largely reduced in deprived serine cells; however, they accumulated immensely in excess serine cells. These specific lipids are more clustered together near the nucleus similar to saturated lipids in both 10x and 20x serine HeLa cells. The control has some unsaturated lipids distributed, but it is more individual and separated compared to other test groups. The distribution of unsaturated lipids is consistent in repeated experiments for all control and serine conditions. **D)** Quantification of unsaturated lipid (3010 cm^{-1}) to total lipid (2850 cm^{-1}) for cancer cells displayed large differences between each condition. ****p<0.001, ***p<0.001, and *p<0.05 from 2-way ANOVA test.

Equivalent to saturated lipids, unsaturated lipids were substantially reduced in 0.25x serine cells but increased in excess serine cells compared to control cells (Figure 2.3C). Thus, total lipids were predominately minimized when cancer cells are deprived with serine but with more available serine, there is an increase in synthesized total lipids which can infer to the accumulation of reactive oxygen species (ROS) (Wang, Palmfeldt et al. 2019, Zhang and Boppart 2021). It has been previously suggested that polyunsaturated lipids are synthesized when ROS is elevated in response to oxidative stress (Wang, Palmfeldt et al. 2019, Cruz, Barreto et al. 2020, Zhang and Boppart 2021). Quantifications of the ratiometric images confirmed that deprived serine reduced unsaturated lipids by 18% while 10x and 20x increase in serine synthesized more lipids by 20% and 35%, respectively (Figure 2.3D). Like saturated lipids, the deprived serine cells show very minimal SRS signal of unsaturated lipids, and the lipid distribution is largely different than the control and surplus of serine in cells. Having an overabundance of serine showed lipids being compacted near the cell's nucleus inferring that the HeLa cells are exhibiting some oxidative stress as they are relying on excess lipids for protection to survive and grow (Wang and Oram 2007, Cruz, Barreto et al. 2020, Zhang and Boppart 2021).

The label-free SRS images displayed that depriving serine from cancer cells resulted in damaged lipid distribution and lower lipid aggregate compared to the control case, whereas adding a surplus of serine will produce greater lipid clusters compacted near the cell's nucleus. Studies have suggested that exogeneous serine is necessary for the synthesis of membrane lipids such as unsaturated and saturated fatty acids as it is an important nutritional intake (Wang and Oram 2007, Esaki, Sayano et al. 2015). Our spontaneous results support this and further show that serine can continue to proliferate cancer further if excess amount is consumed, and there is lipid accumulation taking place with the overabundance of serine (See Supplemental Figure 2.5A). With label-free

SRS imaging, we can confirm our hypothesis in the changes of cancer cell lipid metabolism when serine is being regulated. The ratiometric images and quantifications showed how saturated and unsaturated lipids were enriched in 10x and 20x excess serine, and the cell morphology was larger and more stretched compared to the control and 0.25x deprived serine cells.

2.3.3 SRS Imaging of Protein Metabolic Activity for Varied Concentrations of Serine in Cancer Cells

Resembling lipid metabolism, we wanted to observe how protein was affected by the non-essential amino acid serine in cancer cells. Since we were able to see a significant C-D protein peak in the Spontaneous spectra with significant quantification differences as previously discussed (See Supplemental Figure 2.5B), DO-SRS imaging was applied to observe the newly synthesized proteins for each experimental condition (Figure 2.4A). C-D protein signal is more intense when excess serine is added to cells while depriving serine resulted is almost no new protein synthesis. Compared to control, only 20x excess serine cells showed a higher protein signal by roughly 40% (Figure 2.4B). In contrast, depriving serine from cells reduced *de novo* protein synthesis by approximately 70%, making it remarkably different compared to the control group (Figure 2.4B). These results infer the possibility of autophagy inhibition from mTORC1 activation (Younce and Kolattukudy 2012) and an increase in insulin as the effect of serine has been previously suggested to elevate receptor numbers without changes in affinity (Galbraith and Buse 1981). Upregulation of insulin levels have implied ROS production and oxidative stress in addition to activating other stress-sensitive pathways (Evans, Goldfine et al. 2003, Ceriello and Motz 2004). Our results demonstrated that serine can indeed induce newly synthesized proteins promoting survival and growth in cancer cells.

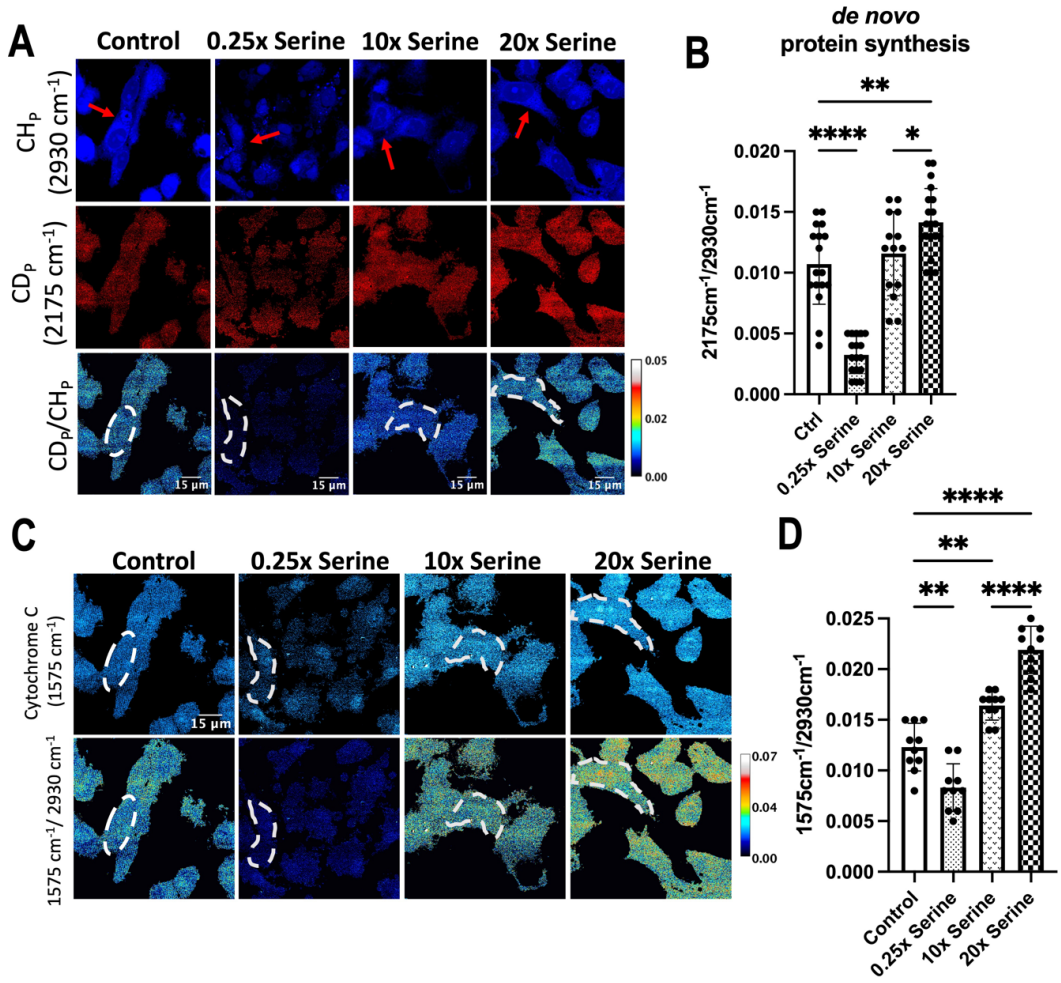

Figure 2.4 SRS images of protein folding and Cytochrome c presence in cancer cells regulated with serine.

A) SRS images of protein metabolic dynamics in HeLa cells. SRS images at 2930 cm^{-1} demonstrate the total (CH) proteins. In the same region of interest, DO-SRS images visualized Deuterium-labelled protein (CD_P) at channel 2175 cm^{-1}. The ratiometric images of CD_P/CH_P were generated to display the newly synthesized proteins. Multiple cell units were selected to calculate the absolute intensities of CD_P/CH_P. **B)** Statistical analysis was performed for the ratiometric images, CD_P/CH_P, to compare the control and experimental conditions which resulted in significant outputs. ****$p<0.0001$, **$p<0.01$, and *$p<0.05$ from performed 2-way ANOVA test. **C)** SRS images of Cytochrome c distribution in HeLa cells were taken at the 1580 cm^{-1} channel. The ratiometric images were evaluated at 1575 cm^{-1}/2930 cm^{-1} to observe Cytochrome c's distribution and concentration. Cytochrome c showed to be evenly distributed in both 10x and 20x serine groups, while its signal level was downregulated in the 0.25x serine condition. 20x serine cells demonstrated to have more evenly distributed Cytochrome c compared to the control and deprived serine group. 10x serine cells have a better distribution of this protein compared to control, but it is more condensed than the 20x serine cells. **D)** Multiple cell units were selected to calculate the absolute intensities of 1575 cm^{-1}/2930 cm^{-1}. Large statistical differences were shown between each experimental condition. ****$p<0.0001$, **$p<0.01$ from 2-way ANOVA test.

Using SRS microscopy, we imaged the Cytochrome c channel in HeLa cells treated with different serine concentration (Figure 2.4C). The spontaneous Raman spectra from Supplemental Figure 2.6A displayed a notable peak at 1575 cm^{-1} indicating the porphyrin ring of Cytochrome c (Kumamoto, Harada et al. 2018, Hniopek, Bocklitz et al. 2021, Li, Bagheri et al. 2022). The ratiometric analysis based on the Raman spectra showed notable differences between the control cells and excess serine cells by approximately 45% and a reduction in protein synthesis by around 20% for 0.25x deprived serine cancer cells (See Supplemental Figure 2.6B). SRS imaging confirmed the Raman spectra results showing similar trends between each experimental condition and the control. We observed the most signal in 10x and 20x serine test groups whereas 0.25x deprived serine cells had almost no signal present. We normalized the intensity of 1575 cm^{-1} to the total protein level at 2930 cm^{-1} in order to analyze the subcellular level of Cytochrome c. As evident in Figure 2.4C, Cytochrome c is clearly present in cells that contain at least 1x serine levels (control) while reduction in serine concentration displays a depletion of this protein. In excess serine cases, Cytochrome c showed a consistent distribution of the protein throughout the cells especially towards the nucleus.

Interestingly, the signal distribution between 10x and 20x excess serine differ significantly which was also verified quantitatively by approximately 35% (Figure 2.4D). Cells with 20x serine concentration showed a more compact formed of Cytochrome c while 10x serine and the control cells showed the protein signal to be more evenly dispersed inferring that Cytochrome c is probable to function in cancer development (Abramczyk, Brozek-Pluska et al. 2022). From our results, a concentration of 20x serine will cause a significant upregulation of Cytochrome c; therefore, resulting in faster cancer progression and cell growth. The notable changes in Cytochrome c levels between each condition demonstrates how mTORC1 regulates the synthesis of proteins when

amino acid levels are modified (Mukaneza, Cohen et al. 2019), and SRS imaging is a useful platform to visualize the metabolic changes and functions of the cells directly.

Cytochrome c has two opposite functions in regards to cancer which include serving as a cell death biomarker in apoptosis and also being an essential protein to sustain life and respiration (Ow, Green et al. 2008). Since Cytochrome c is typically present in the mitochondria, its concentration reflects its contribution to apoptosis and oxidative phosphorylation (Abramczyk, Brozek-Pluska et al. 2022). With the signal being present at 1575 cm^{-1} for HeLa cells, both apoptosis and electron shuttling can take place which ultimately can lead to effective respiration (Vaughn and Deshmukh 2008). The release of Cytochrome c is suggested to cause apoptosis (Abramczyk, Brozek-Pluska et al. 2022) which is why depriving serine from cells causes not only a small signal in the 1575 cm^{-1} channel but also smaller and rounder cells. The evenly distributed Cytochrome c throughout the control and 10x excess serine cells demonstrates possible inflammation and cancer development (Garrido, Galluzzi et al. 2006, Gogvadze, Orrenius et al. 2006). Thus, with SRS imaging, Cytochrome c can be used as a potential biomarker for detecting cellular damage and cell death in cancer diseases.

2.4 Discussion

Previous studies have suggested that many tumors cannot acquire enough serine from their environment (Sullivan, Mattaini et al. 2019, Hennequart, Labuschagne et al. 2021, Tajan, Hennequart et al. 2021, Zhao, Fu et al. 2021). Being a non-essential amino acid, serine derives from nutritional uptake and the serine synthesis pathway which comes from glycolysis (Kalhan and Hanson 2012, Gao, Lee et al. 2018, Hennequart, Labuschagne et al. 2021). Therefore, the variation in serine concentration has a great effect on the proliferation of cancer cells, particularly on lipid and protein metabolism, and understanding how much serine will affect the cell growth

and to what extent is imperative for patient diagnosis and treatment. Spontaneous Raman spectroscopy and SRS microscopy techniques were used to evaluate the metabolic effects of increased and decreased serine in HeLa cells. Heavy water was utilized to track *de novo* lipid and protein synthesis (Figure 2.2A) since carbon-deuterium bonds will produce distinct signals in the spectra's "cell-silent" region (Figure 2.2B). Using SRS imaging, we can recognize how even non-essential amino acids, such as serine, can play a vital role in cancer growth and progression and provide an alternative advance imaging platform to diagnose these diseases more efficiently.

Biomolecules, such as lipids and proteins, have demonstrated to be viable indicators to measure disease progression (Heikal 2010). With DO-SRS, we were able to observe a significant increase in *de novo* lipogenesis when there was an increase in exogenous serine, and a remarkable decrease when cells were deprived from serine compared to the control group (Figure 2.2C). Saturated and unsaturated lipids were visualized at their corresponding wavenumbers to see how this amino acid affected these lipid subtypes (Figure 2.3). Ratiometric images were analyzed and quantified to evaluate a similar trend as the C-D lipids which can infer that serine can cause an oxidative imbalance when there is too much or not enough within cells. The increase in both saturated and unsaturated lipids especially the clusters around the cells when exposed to excess serine can be because the lipid droplets are protecting the cell to promote further progression and proliferation (Jarc and Petan 2019). Indeed, the surplus of lipids is essentially maintaining organelle homeostasis to allow for a longer cell survival and an increase in energy creation (Bailey, Koster et al. 2015). Depriving serine demonstrated a severe reduction in lipids potentially because mTORC1 becomes inactive and AMPK becomes active as a result, so ROS can be accumulated in response to this oxidative stress (Saxton and Sabatini 2017, Zhao, Hu et al. 2017, Mossmann, Park et al. 2018, Wang, Palmfeldt et al. 2019, Zhang and Boppart 2021).

Similar Raman techniques were applied to evaluate how protein metabolism was influenced with changes in serine concentration in HeLa cells. Like lipids, newly synthesized proteins were increased when excess serine was added in culture media compared to the control (Figure 2.4A). Moreover, 0.25x serine in cells downregulated the protein signals significantly for both the C-D and total protein signal. Because mTORC1 is prone to activation from serine oversupply, autophagy becomes inhibited and protein synthesis can increase from oxidative stress taking place, stimulating cancer cell growth (Galbraith and Buse 1981, Younce and Kolattukudy 2012). In addition, Cytochrome c has been shown to be involved in the development of cancer diseases (Abramczyk, Brozek-Pluska et al. 2022), and we were able to observe the Raman peak at 1575 cm^{-1}, which corresponds to Cytochrome c, at different levels with the incorporation of varied serine concentration (See Supplemental Figure 2.6). Using SRS imaging, we visualized how the protein signal was more evenly dispersed between 10x and 20x excess serine cells, meaning that 20x serine concentration could be causing even faster cancer progression as Cytochrome c is highly upregulated (Figure 2.4C). Cytochrome c was minimally present when serine was only present at 0.25x concentration with cells also being smaller in size which could elude to cell death (Nunez, Sancho-Martinez et al. 2010). With Cytochrome c distributed mostly in the mitochondria, its accumulation reflects oxidative phosphorylation and apoptosis (Cai, Yang et al. 1998, Abramczyk, Brozek-Pluska et al. 2022). Our results can conclude that Cytochrome c can be used as a biomarker for cellular damage in cancer, and that manipulating serine will result in either an upregulation or reduction in this protein synthesis.

Overall, our study applies Raman techniques to reveal the effects of lipid and protein metabolism in cancer cells when there is a lack or oversupply of exogenous serine. Using spontaneous Raman, D_2O-probed and label-free SRS imaging, we were able to observe and

confirm our results while also using statistical analysis to evaluate quantitatively how cancer cells were affected with this amino acid. Heavy water allowed us to locate molecules *in situ*, and label-free imaging showed how lipid subtypes and specific proteins directly modify cancer metabolism. Following experiments can potentially look at how different cancer subtypes such as breast cancer metabolism are affected by various serine concentrations. It has been considered that breast cancer cells depend on increased serine that is induced by particular proteins (Possemato, Marks et al. 2011). Furthermore, it would be interesting to observe how environmental signals, such as lack of oxygen, can influence the lipid and protein metabolic dynamics of cancer cells when serine is downregulated in cancer cells. Hypoxic stress is another rationale behind cell death with minimal serine, suggesting that extracellular serine is necessary for cell growth (Engel, Lorenz et al. 2020); however, it is unclear how much serine is required for tumor cells to proliferate and metastasize when exposed to minimal oxygen. Altogether, Raman and DO-SRS imaging have shown to exhibit potential techniques in monitoring the direct metabolic changes in cells that will decipher the functions between metabolism and cancer diseases.

2.5 Supplemental Figures

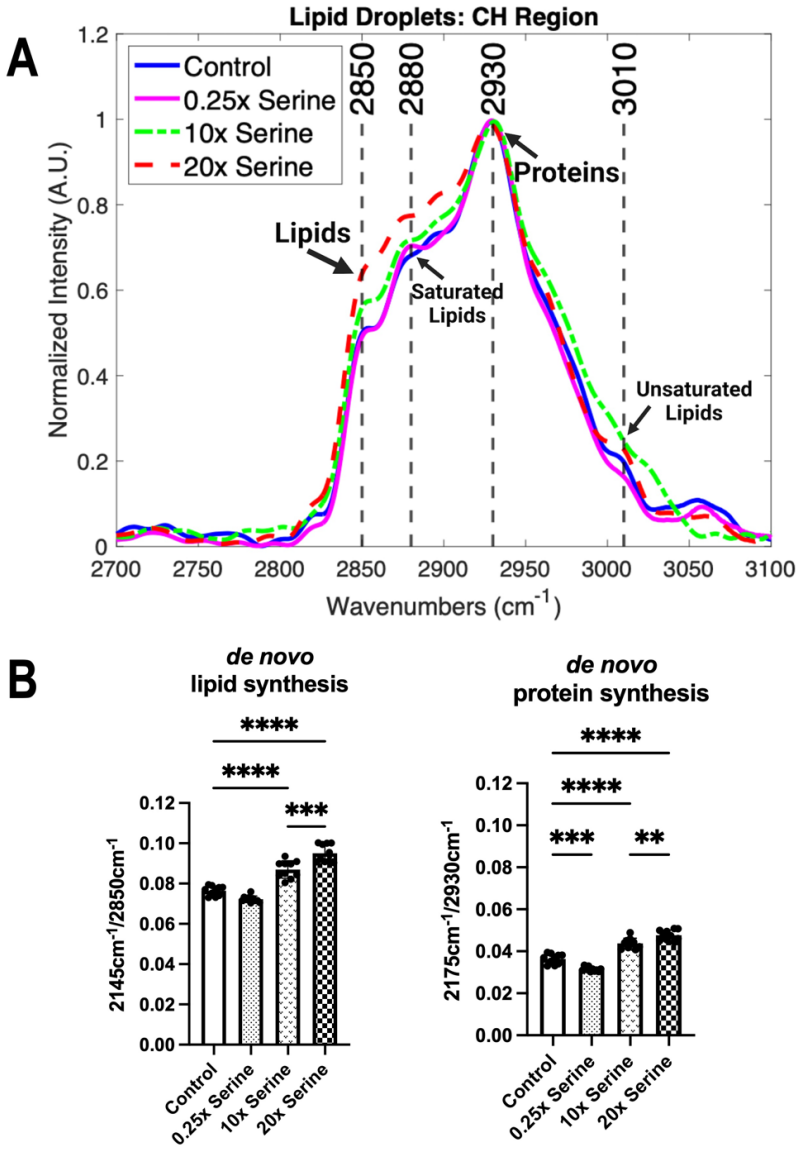

Figure 2.5 Spontaneous Raman spectra using the parameters the following parameters: 90 second acquisition time and accumulation of 3.
A) Raman spectra of the CH region (2700 cm^{-1} – 3100 cm^{-1}) obtained from control and experimental conditions: 0.25x serine, 10x serine, and 20x serine. **B)** Quantifications of the mean ratiometric results from CD_L and CD_P peaks for HeLa un cells under control and regulated serine groups. ****p<0.0001, ***p<00.1, **p<0.01 from 2-way ANOVA test.

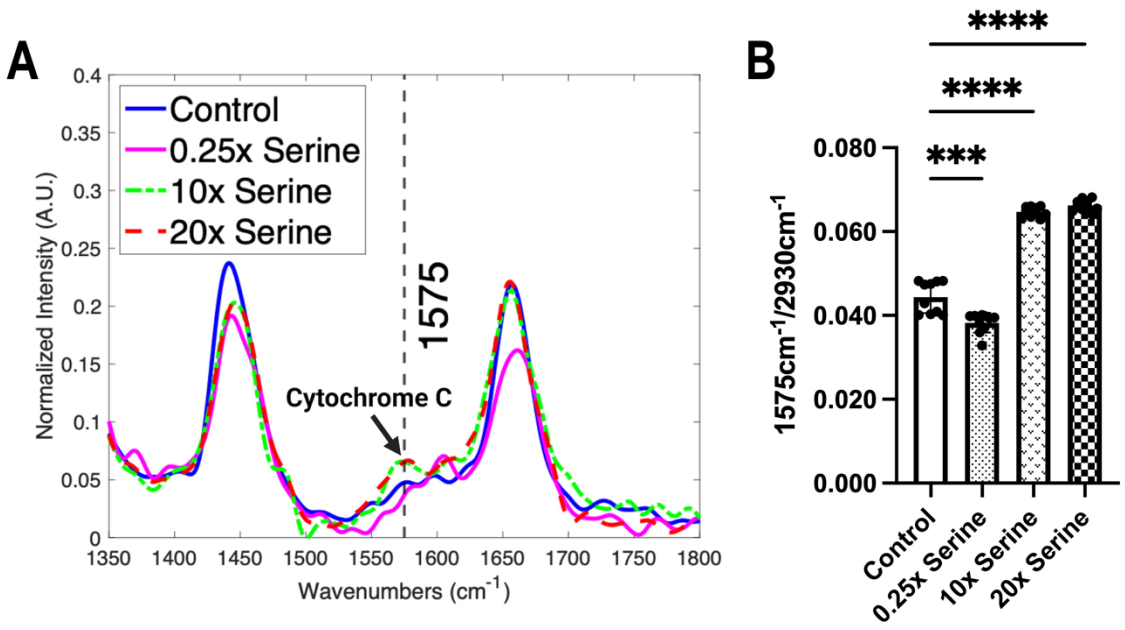

Figure 2.6 Spontaneous Raman spectra ratiometric analysis for Cytochrome c to total protein. A) Spectra showing the peak at 1575 cm^{-1}, corresponding to Cytochrome c for HeLa cells treated under different serine conditions in culture media. B) Quantification of Cytochrome c (1575 cm^{-1}) to total protein (2930 cm^{-1}) for cancer cells shows significant differences between control and deprived and excess serine groups. ****$p<0.001$ and ***$p<0.001$from 2-way ANOVA test.

Chapter 2, in full, is currently being prepared for submission for publications of the material. Bagheri, P.; Shi, L. The thesis author was the primary investigator and author of this material.

CONCLUDING REMARKS AND FUTURE PERSPECTIVE

Various studies in the past years have indicated the impactful roles of amino acids in cancer cell metabolism. Amino acids function in different pathways that can feed cells and provide additional components for cancer cell proliferation. Both essential and nonessential amino acids have shown influences on lipid and protein syntheses in addition to influencing pathways that affect ROS homeostasis and regulation. Inhibiting amino acids has shown to result in successful cancer medications *in vitro*, but challenges for the clinical settings still exist.

With high resolution and sensitivity, the non-invasive imaging technique of Raman scattering spectroscopy/microscopy can be used as an eminent tool and replace common methods such as MS- and MALDI-based spectroscopy for metabolic imaging. With integrations of deuterium oxide probing, we have successfully visualized newly synthesized lipids and proteins in cancer cells and their alterations regulated by amino acids. We are able to gain information such as dynamic tracing and molecular quantifications in more depth compared to other conventional tools. Raman imaging has shown to be a viable early diagnostic imaging technique for complex diseases such as cancer, and Raman modalities are likely to be optimized with higher signal intensity and a larger scale for imaging.

For further investigation of metabolic imaging in cancer cells, the current platforms can be utilized for analyzing how environmental signals, such as the lack of oxygen, influence the metabolic activity of cells. Understanding the interplay between oxygen levels and amino acids is another area of study that has not been visualized closely with these non-invasive techniques. Indeed, it would be interesting to compare different cancer cell lines with the manipulations of amino acids to see if similar results will be present as seen in HeLa cells which would be useful information for clinical applications. On the other hand, this platform can be extended for

differentiating lipid subtypes in cells, by expanding the spectral library of lipid subtypes. This will allow us to unravel the particular lipid subtypes that are regulated by various types of amino acids. We envision broad applications of the SRS and DO-SRS platform for subcellular metabolic imaging for early diagnosis of cancer and other diseases.

REFERENCES

Abramczyk, H., B. Brozek-Pluska and M. Kopec (2022). "Double face of cytochrome c in cancers by Raman imaging." Sci Rep **12**(1): 2120.

Ackerman, D., S. Tumanov, B. Qiu, E. Michalopoulou, M. Spata, A. Azzam, H. Xie, M. C. Simon and J. J. Kamphorst (2018). "Triglycerides Promote Lipid Homeostasis during Hypoxic Stress by Balancing Fatty Acid Saturation." Cell Rep **24**(10): 2596-2605 e2595.

Alhallak, K., L. G. Rebello, T. J. Muldoon, K. P. Quinn and N. Rajaram (2016). "Optical redox ratio identifies metastatic potential-dependent changes in breast cancer cell metabolism." Biomed Opt Express **7**(11): 4364-4374.

Bagheri, P., K. Hoang, A. A. Fung, S. Hussain and L. Shi (2021). "Visualizing Cancer Cell Metabolic Dynamics Regulated With Aromatic Amino Acids Using DO-SRS and 2PEF Microscopy." Front Mol Biosci **8**: 779702.

Bailey, A. P., G. Koster, C. Guillermier, E. M. Hirst, J. I. MacRae, C. P. Lechene, A. D. Postle and A. P. Gould (2015). "Antioxidant Role for Lipid Droplets in a Stem Cell Niche of Drosophila." Cell **163**(2): 340-353.

Berry, D., E. Mader, T. K. Lee, D. Woebken, Y. Wang, D. Zhu, M. Palatinszky, A. Schintlmeister, M. C. Schmid, B. T. Hanson, N. Shterzer, I. Mizrahi, I. Rauch, T. Decker, T. Bocklitz, J. Popp, C. M. Gibson, P. W. Fowler, W. E. Huang and M. Wagner (2015). "Tracking heavy water (D2O) incorporation for identifying and sorting active microbial cells." Proc Natl Acad Sci U S A **112**(2): E194-203.

Blommaart, E. F., J. J. Luiken, P. J. Blommaart, G. M. van Woerkom and A. J. Meijer (1995). "Phosphorylation of ribosomal protein S6 is inhibitory for autophagy in isolated rat hepatocytes." J Biol Chem **270**(5): 2320-2326.

Bowden, N. A., J. P. M. Sanders and M. E. Bruins (2018). "Solubility of the Proteinogenic alpha-Amino Acids in Water, Ethanol, and Ethanol-Water Mixtures." J Chem Eng Data **63**(3): 488-497.

Bowman, A. P., J. F. J. Bogie, J. J. A. Hendriks, M. Haidar, M. Belov, R. M. A. Heeren and S. R. Ellis (2020). "Evaluation of lipid coverage and high spatial resolution MALDI-imaging capabilities of oversampling combined with laser post-ionisation." Anal Bioanal Chem **412**(10): 2277-2289.

Cai, J., J. Yang and D. P. Jones (1998). "Mitochondrial control of apoptosis: the role of cytochrome c." Biochim Biophys Acta **1366**(1-2): 139-149.

Caron, A., D. Richard and M. Laplante (2015). "The Roles of mTOR Complexes in Lipid Metabolism." Annu Rev Nutr **35**: 321-348.

Ceriello, A. and E. Motz (2004). "Is oxidative stress the pathogenic mechanism underlying insulin resistance, diabetes, and cardiovascular disease? The common soil hypothesis revisited." Arterioscler Thromb Vasc Biol **24**(5): 816-823.

Cheng, C., S. Zhuo, B. Zhang, X. Zhao, Y. Liu, C. Liao, J. Quan, Z. Li, A. M. Bode, Y. Cao and X. Luo (2019). "Treatment implications of natural compounds targeting lipid metabolism in nonalcoholic fatty liver disease, obesity and cancer." Int J Biol Sci **15**(8): 1654-1663.

Chiacchiera, F. and C. Simone (2009). "Inhibition of p38alpha unveils an AMPK-FoxO3A axis linking autophagy to cancer-specific metabolism." Autophagy **5**(7): 1030-1033.

Choe, C., J. Lademann and M. E. Darvin (2016). "A depth-dependent profile of the lipid conformation and lateral packing order of the stratum corneum in vivo measured using Raman microscopy." Analyst **141**(6): 1981-1987.

Cruz, A. L. S., E. A. Barreto, N. P. B. Fazolini, J. P. B. Viola and P. T. Bozza (2020). "Lipid droplets: platforms with multiple functions in cancer hallmarks." Cell Death Dis **11**(2): 105.

Da Silva, E., S. Bresson and D. Rousseau (2009). "Characterization of the three major polymorphic forms and liquid state of tristearin by Raman spectroscopy." Chem Phys Lipids **157**(2): 113-119.

Daudon, M. B., D. (2016). "Vibrational spectroscopies to investigate concretions and ectopic calcifications for medical diagnosis." Comptes Rendus Chimie **19**(11-12): 1416-1423.

de la Cruz López, K. G., M. E. Toledo Guzmán, E. O. Sánchez and A. García Carrancá (2019). "mTORC1 as a Regulator of Mitochondrial Functions and a Therapeutic Target in Cancer." Frontiers in Oncology **9**(1373).

Di Gialleonardo, V., D. M. Wilson and K. R. Keshari (2016). "The Potential of Metabolic Imaging." Semin Nucl Med **46**(1): 28-39.

Ember, K. J. I., M. A. Hoeve, S. L. McAughtrie, M. S. Bergholt, B. J. Dwyer, M. M. Stevens, K. Faulds, S. J. Forbes and C. J. Campbell (2017). "Raman spectroscopy and regenerative medicine: a review." NPJ Regen Med **2**: 12.

Engel, A. L., N. I. Lorenz, K. Klann, C. Munch, C. Depner, J. P. Steinbach, M. W. Ronellenfitsch and A. L. Luger (2020). "Serine-dependent redox homeostasis regulates glioblastoma cell survival." Br J Cancer **122**(9): 1391-1398.

Esaki, K., T. Sayano, C. Sonoda, T. Akagi, T. Suzuki, T. Ogawa, M. Okamoto, T. Yoshikawa, Y. Hirabayashi and S. Furuya (2015). "L-Serine Deficiency Elicits Intracellular Accumulation of Cytotoxic Deoxysphingolipids and Lipid Body Formation." J Biol Chem **290**(23): 14595-14609.

Evans, J. L., I. D. Goldfine, B. A. Maddux and G. M. Grodsky (2003). "Are oxidative stress-activated signaling pathways mediators of insulin resistance and beta-cell dysfunction?" Diabetes **52**(1): 1-8.

Fingar, D. C., S. Salama, C. Tsou, E. Harlow and J. Blenis (2002). "Mammalian cell size is controlled by mTOR and its downstream targets S6K1 and 4EBP1/eIF4E." Genes Dev **16**(12): 1472-1487.

Fung, A. A. and L. Shi (2020). "Mammalian cell and tissue imaging using Raman and coherent Raman microscopy." Wiley Interdiscip Rev Syst Biol Med **12**(6): e1501.

Galbraith, R. A. and M. G. Buse (1981). "Effects of serine on protein synthesis and insulin receptors." Am J Physiol **241**(3): C167-171.

Gao, X., K. Lee, M. A. Reid, S. M. Sanderson, C. Qiu, S. Li, J. Liu and J. W. Locasale (2018). "Serine Availability Influences Mitochondrial Dynamics and Function through Lipid Metabolism." Cell Rep **22**(13): 3507-3520.

Garrido, C., L. Galluzzi, M. Brunet, P. E. Puig, C. Didelot and G. Kroemer (2006). "Mechanisms of cytochrome c release from mitochondria." Cell Death Differ **13**(9): 1423-1433.

Geeraert, C., A. Ratier, S. G. Pfisterer, D. Perdiz, I. Cantaloube, A. Rouault, S. Pattingre, T. Proikas-Cezanne, P. Codogno and C. Pous (2010). "Starvation-induced hyperacetylation of tubulin is required for the stimulation of autophagy by nutrient deprivation." J Biol Chem **285**(31): 24184-24194.

Ghita, A., F. C. Pascut, M. Mather, V. Sottile and I. Notingher (2012). "Cytoplasmic RNA in undifferentiated neural stem cells: a potential label-free Raman spectral marker for assessing the undifferentiated status." Anal Chem **84**(7): 3155-3162.

Ghosh, J. and R. Kapur (2017). "Role of mTORC1-S6K1 signaling pathway in regulation of hematopoietic stem cell and acute myeloid leukemia." Exp Hematol **50**: 13-21.

Gogvadze, V., S. Orrenius and B. Zhivotovsky (2006). "Multiple pathways of cytochrome c release from mitochondria in apoptosis." Biochim Biophys Acta **1757**(5-6): 639-647.

Guridi, M., B. Kupr, K. Romanino, S. Lin, D. Falcetta, L. Tintignac and M. A. Ruegg (2016). "Alterations to mTORC1 signaling in the skeletal muscle differentially affect whole-body metabolism." Skelet Muscle **6**: 13.

Hardie, D. G. (2007). "AMP-activated/SNF1 protein kinases: conserved guardians of cellular energy." Nat Rev Mol Cell Biol **8**(10): 774-785.

Heikal, A. A. (2010). "Intracellular coenzymes as natural biomarkers for metabolic activities and mitochondrial anomalies." Biomark Med **4**(2): 241-263.

Hennequart, M., C. F. Labuschagne, M. Tajan, S. E. Pilley, E. C. Cheung, N. M. Legrave, P. C. Driscoll and K. H. Vousden (2021). "The impact of physiological metabolite levels on serine uptake, synthesis and utilization in cancer cells." Nat Commun **12**(1): 6176.

Herms, A., M. Bosch, B. J. Reddy, N. L. Schieber, A. Fajardo, C. Ruperez, A. Fernandez-Vidal, C. Ferguson, C. Rentero, F. Tebar, C. Enrich, R. G. Parton, S. P. Gross and A. Pol (2015). "AMPK activation promotes lipid droplet dispersion on detyrosinated microtubules to increase mitochondrial fatty acid oxidation." Nat Commun **6**: 7176.

Hniopek, J., T. Bocklitz, M. Schmitt and J. Popp (2021). "Probing Protein Secondary Structure Influence on Active Centers with Hetero Two-Dimensional Correlation (Resonance) Raman Spectroscopy: A Demonstration on Cytochrome C." Appl Spectrosc **75**(8): 1043-1052.

Jamieson, L. E., A. Li, K. Faulds and D. Graham (2018). "Ratiometric analysis using Raman spectroscopy as a powerful predictor of structural properties of fatty acids." R Soc Open Sci **5**(12): 181483.

Jarc, E. and T. Petan (2019). "Lipid Droplets and the Management of Cellular Stress." Yale J Biol Med **92**(3): 435-452.

Jones, R. G., D. R. Plas, S. Kubek, M. Buzzai, J. Mu, Y. Xu, M. J. Birnbaum and C. B. Thompson (2005). "AMP-activated protein kinase induces a p53-dependent metabolic checkpoint." Mol Cell **18**(3): 283-293.

Kalhan, S. C. and R. W. Hanson (2012). "Resurgence of serine: an often neglected but indispensable amino Acid." J Biol Chem **287**(24): 19786-19791.

Khatchadourian, A., S. D. Bourque, V. R. Richard, V. I. Titorenko and D. Maysinger (2012). "Dynamics and regulation of lipid droplet formation in lipopolysaccharide (LPS)-stimulated microglia." Biochim Biophys Acta **1821**(4): 607-617.

Kimura, T. and Y. Watanabe (2016). "Tryptophan protects hepatocytes against reactive oxygen species-dependent cell death via multiple pathways including Nrf2-dependent gene induction." Amino Acids **48**(5): 1263-1274.

Kumamoto, Y., Y. Harada, T. Takamatsu and H. Tanaka (2018). "Label-free Molecular Imaging and Analysis by Raman Spectroscopy." Acta Histochem Cytochem **51**(3): 101-110.

Lee, S. J., J. Zhang, A. M. Choi and H. P. Kim (2013). "Mitochondrial dysfunction induces formation of lipid droplets as a generalized response to stress." Oxid Med Cell Longev **2013**: 327167.

Li, X., M. Jiang, J. W. Y. Lam, B. Z. Tang and J. Y. Qu (2017). "Mitochondrial Imaging with Combined Fluorescence and Stimulated Raman Scattering Microscopy Using a Probe of the Aggregation-Induced Emission Characteristic." J Am Chem Soc **139**(47): 17022-17030.

Li, Y., P. Bagheri, P. Chang, A. Zeng, J. Hao, A. Fung, J. Y. Wu and L. Shi (2022). "Direct Imaging of Lipid Metabolic Changes in Drosophila Ovary During Aging Using DO-SRS Microscopy." Frontiers in Aging **2**.

Li, Y., W. Zhang, A. A. Fung and L. Shi (2021). "DO-SRS imaging of metabolic dynamics in aging Drosophila." Analyst **146**(24): 7510-7519.

Li, Z., S. Cheng, Q. Lin, W. Cao, J. Yang, M. Zhang, A. Shen, W. Zhang, Y. Xia, X. Ma and Z. Ouyang (2021). "Single-cell lipidomics with high structural specificity by mass spectrometry." Nat Commun **12**(1): 2869.

Lieu, E. L., T. Nguyen, S. Rhyne and J. Kim (2020). "Amino acids in cancer." Exp Mol Med **52**(1): 15-30.

Lisec, J., C. Jaeger, R. Rashid, R. Munir and N. Zaidi (2019). "Cancer cell lipid class homeostasis is altered under nutrient-deprivation but stable under hypoxia." BMC Cancer **19**(1): 501.

Ma, Q., J. Chen, X. Zhou, L. Hu, Y. Sun, Z. Wang, Z. Yue and A. Shan (2021). "Dietary supplementation with aromatic amino acids decreased triglycerides and alleviated hepatic steatosis by stimulating bile acid synthesis in mice." Food Funct **12**(1): 267-277.

Maddocks, O. D. K., D. Athineos, E. C. Cheung, P. Lee, T. Zhang, N. J. F. van den Broek, G. M. Mackay, C. F. Labuschagne, D. Gay, F. Kruiswijk, J. Blagih, D. F. Vincent, K. J. Campbell, F. Ceteci, O. J. Sansom, K. Blyth and K. H. Vousden (2017). "Modulating the therapeutic response of tumours to dietary serine and glycine starvation." Nature **544**(7650): 372-376.

Mahou, P., M. Zimmerley, K. Loulier, K. S. Matho, G. Labroille, X. Morin, W. Supatto, J. Livet, D. Debarre and E. Beaurepaire (2012). "Multicolor two-photon tissue imaging by wavelength mixing." Nat Methods **9**(8): 815-818.

Marcinkiewicz, A., D. Gauthier, A. Garcia and D. L. Brasaemle (2006). "The phosphorylation of serine 492 of perilipin a directs lipid droplet fragmentation and dispersion." J Biol Chem **281**(17): 11901-11909.

Matthews, Q., A. Jirasek, J. Lum, X. Duan and A. G. Brolo (2010). "Variability in Raman spectra of single human tumor cells cultured in vitro: correlation with cell cycle and culture confluency." Appl Spectrosc **64**(8): 871-887.

Mayevsky, A. and E. Barbiro-Michaely (2009). "Use of NADH fluorescence to determine mitochondrial function in vivo." Int J Biochem Cell Biol **41**(10): 1977-1988.

Min, W., C. W. Freudiger, S. Lu and X. S. Xie (2011). "Coherent nonlinear optical imaging: beyond fluorescence microscopy." Annu Rev Phys Chem **62**: 507-530.

Miyagi, M. and T. Kasumov (2016). "Monitoring the synthesis of biomolecules using mass spectrometry." Philos Trans A Math Phys Eng Sci **374**(2079).

Moneim, A. E. (2015). "Oxidant/Antioxidant imbalance and the risk of Alzheimer's disease." Curr Alzheimer Res **12**(4): 335-349.

Mossmann, D., S. Park and M. N. Hall (2018). "mTOR signalling and cellular metabolism are mutual determinants in cancer." Nat Rev Cancer **18**(12): 744-757.

Mukaneza, Y., A. Cohen, M. E. Rivard, J. Tardif, S. Deschenes, M. Ruiz, L. Consortium, C. Laprise, C. Des Rosiers and L. Coderre (2019). "mTORC1 is required for expression of LRPPRC and cytochrome-c oxidase but not HIF-1alpha in Leigh syndrome French Canadian type patient fibroblasts." Am J Physiol Cell Physiol **317**(1): C58-C67.

Munir, R., J. Lisec, J. V. Swinnen and N. Zaidi (2019). "Lipid metabolism in cancer cells under metabolic stress." Br J Cancer **120**(12): 1090-1098.

Murphy, R. C., J. A. Hankin and R. M. Barkley (2009). "Imaging of lipid species by MALDI mass spectrometry." J Lipid Res **50 Suppl**: S317-322.

Muthusamy, T., T. Cordes, M. K. Handzlik, L. You, E. W. Lim, J. Gengatharan, A. F. M. Pinto, M. G. Badur, M. J. Kolar, M. Wallace, A. Saghatelian and C. M. Metallo (2020). "Serine restriction alters sphingolipid diversity to constrain tumour growth." Nature **586**(7831): 790-795.

Nguyen, T. B., S. M. Louie, J. R. Daniele, Q. Tran, A. Dillin, R. Zoncu, D. K. Nomura and J. A. Olzmann (2017). "DGAT1-Dependent Lipid Droplet Biogenesis Protects Mitochondrial Function during Starvation-Induced Autophagy." Dev Cell **42**(1): 9-21 e25.

Nunez, R., S. M. Sancho-Martinez, J. M. Novoa and F. J. Lopez-Hernandez (2010). "Apoptotic volume decrease as a geometric determinant for cell dismantling into apoptotic bodies." Cell Death Differ **17**(11): 1665-1671.

Ow, Y. P., D. R. Green, Z. Hao and T. W. Mak (2008). "Cytochrome c: functions beyond respiration." Nat Rev Mol Cell Biol **9**(7): 532-542.

Paquette, M., L. El-Houjeiri, C. Z. L, P. Puustinen, P. Blanchette, H. Jeong, K. Dejgaard, P. M. Siegel and A. Pause (2021). "AMPK-dependent phosphorylation is required for transcriptional activation of TFEB and TFE3." Autophagy: 1-19.

Parthasarathy, A., P. J. Cross, R. C. J. Dobson, L. E. Adams, M. A. Savka and A. O. Hudson (2018). "A Three-Ring Circus: Metabolism of the Three Proteogenic Aromatic Amino Acids and Their Role in the Health of Plants and Animals." Front Mol Biosci **5**: 29.

Pavlova, N. N. and C. B. Thompson (2016). "The Emerging Hallmarks of Cancer Metabolism." Cell Metab **23**(1): 27-47.

Phillips, M. M., M. T. Sheaff and P. W. Szlosarek (2013). "Targeting arginine-dependent cancers with arginine-degrading enzymes: opportunities and challenges." Cancer Res Treat **45**(4): 251-262.

Pirman, D. A., E. Efuet, X. P. Ding, Y. Pan, L. Tan, S. M. Fischer, R. N. DuBois and P. Yang (2013). "Changes in cancer cell metabolism revealed by direct sample analysis with MALDI mass spectrometry." PLoS One **8**(4): e61379.

Polet, F., C. Corbet, A. Pinto, L. I. Rubio, R. Martherus, V. Bol, X. Drozak, V. Gregoire, O. Riant and O. Feron (2016). "Reducing the serine availability complements the inhibition of the glutamine metabolism to block leukemia cell growth." Oncotarget **7**(2): 1765-1776.

Porporato, P. E., N. Filigheddu, J. M. B. Pedro, G. Kroemer and L. Galluzzi (2018). "Mitochondrial metabolism and cancer." Cell Res **28**(3): 265-280.

Possemato, R., K. M. Marks, Y. D. Shaul, M. E. Pacold, D. Kim, K. Birsoy, S. Sethumadhavan, H. K. Woo, H. G. Jang, A. K. Jha, W. W. Chen, F. G. Barrett, N. Stransky, Z. Y. Tsun, G. S. Cowley, J. Barretina, N. Y. Kalaany, P. P. Hsu, K. Ottina, A. M. Chan, B. Yuan, L. A. Garraway, D. E. Root, M. Mino-Kenudson, E. F. Brachtel, E. M. Driggers and D. M. Sabatini (2011). "Functional genomics reveal that the serine synthesis pathway is essential in breast cancer." Nature **476**(7360): 346-350.

Ralhan, I., C. L. Chang, J. Lippincott-Schwartz and M. S. Ioannou (2021). "Lipid droplets in the nervous system." J Cell Biol **220**(7).

Reuter, S., S. C. Gupta, M. M. Chaturvedi and B. B. Aggarwal (2010). "Oxidative stress, inflammation, and cancer: how are they linked?" Free Radic Biol Med **49**(11): 1603-1616.

Rossi, G., V. Redaelli, P. Contiero, S. Fabiano, G. Tagliabue, P. Perego, L. Benussi, A. C. Bruni, G. Filippini, M. Farinotti, G. Giaccone, S. Buiatiotis, C. Manzoni, R. Ferrari and F. Tagliavini (2018). "Tau Mutations Serve as a Novel Risk Factor for Cancer." Cancer Research **78**(13): 3731-3739.

Rysman, E., K. Brusselmans, K. Scheys, L. Timmermans, R. Derua, S. Munck, P. P. Van Veldhoven, D. Waltregny, V. W. Daniels, J. Machiels, F. Vanderhoydonc, K. Smans, E. Waelkens, G. Verhoeven and J. V. Swinnen (2010). "De novo lipogenesis protects cancer cells from free radicals and chemotherapeutics by promoting membrane lipid saturation." Cancer Res **70**(20): 8117-8126.

Saha, S. K., S. B. Lee, J. Won, H. Y. Choi, K. Kim, G. M. Yang, A. A. Dayem and S. G. Cho (2017). "Correlation between Oxidative Stress, Nutrition, and Cancer Initiation." Int J Mol Sci **18**(7).

Sancak, Y., L. Bar-Peled, R. Zoncu, A. L. Markhard, S. Nada and D. M. Sabatini (2010). "Ragulator-Rag complex targets mTORC1 to the lysosomal surface and is necessary for its activation by amino acids." Cell **141**(2): 290-303.

Saxton, R. A. and D. M. Sabatini (2017). "mTOR Signaling in Growth, Metabolism, and Disease." Cell **168**(6): 960-976.

Saxton, R. A. and D. M. Sabatini (2017). "mTOR Signaling in Growth, Metabolism, and Disease." Cell **169**(2): 361-371.

Schott, M. B., S. G. Weller, R. J. Schulze, E. W. Krueger, K. Drizyte-Miller, C. A. Casey and M. A. McNiven (2019). "Lipid droplet size directs lipolysis and lipophagy catabolism in hepatocytes." J Cell Biol **218**(10): 3320-3335.

Sengupta, S., T. R. Peterson and D. M. Sabatini (2010). "Regulation of the mTOR complex 1 pathway by nutrients, growth factors, and stress." Mol Cell **40**(2): 310-322.

Shi, L., Y. Shen and W. Min (2018). "Invited Article: Visualizing protein synthesis in mice with in vivo labeling of deuterated amino acids using vibrational imaging." APL Photonics **3**(9): 092401.

Shi, L., C. Zheng, Y. Shen, Z. Chen, E. S. Silveira, L. Zhang, M. Wei, C. Liu, C. de Sena-Tomas, K. Targoff and W. Min (2018). "Optical imaging of metabolic dynamics in animals." Nat Commun **9**(1): 2995.

Sullivan, M. R., K. R. Mattaini, E. A. Dennstedt, A. A. Nguyen, S. Sivanand, M. F. Reilly, K. Meeth, A. Muir, A. M. Darnell, M. W. Bosenberg, C. A. Lewis and M. G. Vander Heiden (2019). "Increased Serine Synthesis Provides an Advantage for Tumors Arising in Tissues Where Serine Levels Are Limiting." Cell Metab **29**(6): 1410-1421 e1414.

Surre, J., C. Saint-Ruf, V. Collin, S. Orenga, M. Ramjeet and I. Matic (2018). "Strong increase in the autofluorescence of cells signals struggle for survival." Sci Rep **8**(1): 12088.

Sztalryd, C. and D. L. Brasaemle (2017). "The perilipin family of lipid droplet proteins: Gatekeepers of intracellular lipolysis." Biochim Biophys Acta Mol Cell Biol Lipids **1862**(10 Pt B): 1221-1232.

Tajan, M., M. Hennequart, E. C. Cheung, F. Zani, A. K. Hock, N. Legrave, O. D. K. Maddocks, R. A. Ridgway, D. Athineos, A. Suarez-Bonnet, R. L. Ludwig, L. Novellasdemunt, N. Angelis, V. S. W. Li, G. Vlachogiannis, N. Valeri, N. Mainolfi, V. Suri, A. Friedman, M. Manfredi, K. Blyth, O. J. Sansom and K. H. Vousden (2021). "Serine synthesis pathway inhibition cooperates with dietary serine and glycine limitation for cancer therapy." Nat Commun **12**(1): 366.

Takahara, T., Y. Amemiya, R. Sugiyama, M. Maki and H. Shibata (2020). "Amino acid-dependent control of mTORC1 signaling: a variety of regulatory modes." J Biomed Sci **27**(1): 87.

Thiam, A. R. and M. Beller (2017). "The why, when and how of lipid droplet diversity." J Cell Sci **130**(2): 315-324.

Thiam, A. R. and I. Dugail (2019). "Lipid droplet-membrane contact sites - from protein binding to function." J Cell Sci **132**(12).

Thiem, S., T. P. Pierce, M. Palmieri, T. L. Putoczki, M. Buchert, A. Preaudet, R. O. Farid, C. Love, B. Catimel, Z. Lei, S. Rozen, V. Gopalakrishnan, F. Schaper, M. Hallek, A. Boussioutas, P. Tan, A. Jarnicki and M. Ernst (2013). "mTORC1 inhibition restricts inflammation-associated gastrointestinal tumorigenesis in mice." J Clin Invest **123**(2): 767-781.

Tomar, D., F. Jana, Z. Dong, W. J. Quinn, 3rd, P. Jadiya, S. L. Breves, C. C. Daw, S. Srikantan, S. Shanmughapriya, N. Nemani, E. Carvalho, A. Tripathi, A. M. Worth, X. Zhang, R. Razmpour, A. Seelam, S. Rhode, A. V. Mehta, M. Murray, D. Slade, S. H. Ramirez, P. Mishra, G. S. Gerhard, J. Caplan, L. Norton, K. Sharma, S. Rajan, D. Balciunas, D. S. Wijesinghe, R. S. Ahima, J. A. Baur and M. Madesh (2019). "Blockade of MCU-Mediated Ca(2+) Uptake Perturbs Lipid Metabolism via PP4-Dependent AMPK Dephosphorylation." Cell Rep **26**(13): 3709-3725 e3707.

Uematsu, M. and T. Shimizu (2021). "Raman microscopy-based quantification of the physical properties of intracellular lipids." Commun Biol **4**(1): 1176.

Vadlakonda, L., A. Dash, M. Pasupuleti, K. Anil Kumar and P. Reddanna (2013). "The Paradox of Akt-mTOR Interactions." Front Oncol **3**: 165.

van Manen, H. J., A. Lenferink and C. Otto (2008). "Noninvasive imaging of protein metabolic labeling in single human cells using stable isotopes and Raman microscopy." Anal Chem **80**(24): 9576-9582.

Vaughn, A. E. and M. Deshmukh (2008). "Glucose metabolism inhibits apoptosis in neurons and cancer cells by redox inactivation of cytochrome c." Nat Cell Biol **10**(12): 1477-1483.

Wang, H., Y. Ji, G. Wu, K. Sun, Y. Sun, W. Li, B. Wang, B. He, Q. Zhang, Z. Dai and Z. Wu (2015). "l-Tryptophan Activates Mammalian Target of Rapamycin and Enhances Expression of Tight Junction Proteins in Intestinal Porcine Epithelial Cells." J Nutr **145**(6): 1156-1162.

Wang, T., H. Shogomori, M. Hara, T. Yamada and T. Kobayashi (2012). "Nanomechanical recognition of sphingomyelin-rich membrane domains by atomic force microscopy." Biochemistry **51**(1): 74-82.

Wang, Y. and J. F. Oram (2007). "Unsaturated fatty acids phosphorylate and destabilize ABCA1 through a protein kinase C delta pathway." J Lipid Res **48**(5): 1062-1068.

Wang, Y., J. Palmfeldt, N. Gregersen, A. M. Makhov, J. F. Conway, M. Wang, S. P. McCalley, S. Basu, H. Alharbi, C. St Croix, M. J. Calderon, S. Watkins and J. Vockley (2019). "Mitochondrial fatty acid oxidation and the electron transport chain comprise a multifunctional mitochondrial protein complex." J Biol Chem **294**(33): 12380-12391.

Watmough, N. J., L. A. Bindoff, M. A. Birch-Machin, S. Jackson, K. Bartlett, C. I. Ragan, J. Poulton, R. M. Gardiner, H. S. Sherratt and D. M. Turnbull (1990). "Impaired mitochondrial beta-oxidation in a patient with an abnormality of the respiratory chain. Studies in skeletal muscle mitochondria." J Clin Invest **85**(1): 177-184.

Wei, Z., X. Liu, C. Cheng, W. Yu and P. Yi (2020). "Metabolism of Amino Acids in Cancer." Front Cell Dev Biol **8**: 603837.

Woodcock, H. V., J. D. Eley, D. Guillotin, M. Plate, C. B. Nanthakumar, M. Martufi, S. Peace, G. Joberty, D. Poeckel, R. B. Good, A. R. Taylor, N. Zinn, M. Redding, E. J. Forty, R. E. Hynds, C. Swanton, M. Karsdal, T. M. Maher, A. Fisher, G. Bergamini, R. P. Marshall, A. D. Blanchard, P. F. Mercer and R. C. Chambers (2020). "Author Correction: The mTORC1/4E-BP1 axis represents a critical signaling node during fibrogenesis." Nat Commun **11**(1): 4680.

Wu, G. (2013). "Functional amino acids in nutrition and health." Amino Acids **45**(3): 407-411.

Yamakoshi, H., K. Dodo, M. Okada, J. Ando, A. Palonpon, K. Fujita, S. Kawata and M. Sodeoka (2011). "Imaging of EdU, an alkyne-tagged cell proliferation probe, by Raman microscopy." J Am Chem Soc **133**(16): 6102-6105.

Yang, H., X. Jiang, B. Li, H. J. Yang, M. Miller, A. Yang, A. Dhar and N. P. Pavletich (2017). "Mechanisms of mTORC1 activation by RHEB and inhibition by PRAS40." Nature **552**(7685): 368-373.

Yang, M. and K. H. Vousden (2016). "Serine and one-carbon metabolism in cancer." Nat Rev Cancer **16**(10): 650-662.

Younce, C. and P. Kolattukudy (2012). "MCP-1 induced protein promotes adipogenesis via oxidative stress, endoplasmic reticulum stress and autophagy." Cell Physiol Biochem **30**(2): 307-320.

Yun, C. W. and S. H. Lee (2018). "The Roles of Autophagy in Cancer." Int J Mol Sci **19**(11).

Zhang, C. and S. A. Boppart (2021). "Tracking the formation and degradation of fatty-acid-accumulated mitochondria using label-free chemical imaging." Sci Rep **11**(1): 6671.

Zhang, L., L. Shi, Y. Shen, Y. Miao, M. Wei, N. Qian, Y. Liu and W. Min (2019). "Spectral tracing of deuterium for imaging glucose metabolism." Nat Biomed Eng **3**(5): 402-413.

Zhang, X., T. D. Evans, S. J. Jeong and B. Razani (2018). "Classical and alternative roles for autophagy in lipid metabolism." Curr Opin Lipidol **29**(3): 203-211.

Zhao, X., J. Fu, B. Hu, L. Chen, J. Wang, J. Fang, C. Ge, H. Lin, K. Pan, L. Fu, L. Wang, J. Du and W. Xu (2021). "Serine Metabolism Regulates YAP Activity Through USP7 in Colon Cancer." Front Cell Dev Biol **9**: 639111.

Zhao, Y., X. Hu, Y. Liu, S. Dong, Z. Wen, W. He, S. Zhang, Q. Huang and M. Shi (2017). "ROS signaling under metabolic stress: cross-talk between AMPK and AKT pathway." Mol Cancer **16**(1): 79.

Zhao, Z., C. Chen, H. Xiong, J. Ji and W. Min (2020). "Metabolic Activity Phenotyping of Single Cells with Multiplexed Vibrational Probes." Anal Chem **92**(14): 9603-9612.